JOURNAL OF MATERIALS SCIENCE 29 (1994) 4135–4151

Review
Bismuth oxide-based solid electrolytes for fuel cells

A. M. AZAD, S. LAROSE, S. A. AKBAR
Department of Materials Science and Engineering, The Ohio State University, Columbus, OH 43210, USA

During the last three decades, a large number of investigations has been reported pertaining to the science and technology of solid oxide fuel cells (SOFCs) based mainly on the yttria-stabilized zirconia (YSZ) electrolyte. Because of the problems associated with the high temperature of operation (~ 1000 °C) of the YSZ-based cells, there has been a substantial effort to develop alternative electrolytes with ionic conductivity comparable to that of YSZ at relatively lower temperatures. This review presents a systematic evolution in the area of the development of new electrolytes based on bismuth sesquioxide for fuel cell applications at moderate temperatures.

1. Introduction

The modern scientific and technological approach in the area of energy production is to develop inexpensive devices, which would satisfy the current drive for cleaner and more efficiently distributed power, particularly in combined heat and power systems. In this context, fuel cells represent a promising and viable alternative for large-scale generation of electricity, with minimal undesirable chemical, thermal and acoustic emissions. A fuel cell is a device that directly converts the chemical energy of reactants (a fuel such as hydrogen, natural gas, methane or methanol, and an oxidant, air or oxygen), into low-voltage d.c. electricity. Fuel cells are often classified according to the kind of electrolyte they incorporate and also the temperature range of their operation. Among the initially developed devices, the widely used ones are the low-temperature phosphoric acid fuel cells [1] and those based on aqueous alkaline electrolytes [2]. However, the aqueous electrolytes may flood the porous electrodes, evaporate, undergo compositional changes, decompose and eventually lead to poor performance. Attempts to overcome some or all of these shortcomings would result in a rather complex design. Moreover, because the relatively low temperature of operation restrains the kinetics, expensive platinum-based catalysts are used at the electrolyte–electrode interface.

The fuel cells operating at elevated temperatures (~ 700 °C or above) employ either a mixed molten carbonate or ceramic solid oxide as the electrolyte and are accordingly known as the molten carbonate fuel cells (MCFCs) and the solid oxide fuel cells (SOFCs), respectively. Some of the salient characteristics of these two types of fuel cells are compared in Table I. Both these devices can use hydrocarbon fuels, reformed internally on the electrodes, with ordinary air as the oxidant; both are of comparable efficiencies, which are higher than those of Carnot heat engines, and both are cool enough to prevent NO_x formation [3]. The main distinction between the two cells, however, lies in the choice of electrolyte. Obviously, a system having molten salt as the working medium is more prone to creep and corrosion than metals and ceramics. On the other hand, a ceramic-based system is subjected to the risk of thermal shock and undesirable gas permeation. Nevertheless, there have been major improvements in the development of fuel cells, and the long-term stability of single cells has been demonstrated. Recently, Minh [4, 5] has exhaustively discussed and reviewed the critical issues pertaining to the science and technology of ceramic fuel cells. The emphasis was given to the zirconia electrolyte, anode, cathode, interconnect material, design and processing techniques and the electrode reactions involving gaseous fuels.

SOFCs have an edge over MCFCs in that [6–8]:

(a) they allow the fuel cells to run at higher temperatures;
(b) expensive precious metal catalysts are not needed to promote reaction between hydrogen and oxygen;
(c) methane is readily reformed into hydrogen and carbon monoxide; and
(d) the waste heat from the cell is useful in powering heaters, boilers and air conditioners.

It is interesting to note that at the upper end of its temperature range, unlike the MCFC, SOFC is an all-ceramic system, which signifies the prospect of miniaturization of the device without sacrificing the efficiency. Miniaturization principally stems from the availability of the well-developed techniques of thick- and thin-film printing, where the components could be laid in microlayered structures. Another advantage of

0022–2461

TABLE I Comparison of solid oxide fuel cells (SOFCs) and molten carbonate fuel cells (MCFCs)

Property/ characteristic	SOFC	MCFC
Electrolyte	YSZ	Lithium/potassium carbonate
Fuel	Methane/ methanol	Methane/methanol
Oxidant	Air	Air
Pressure (atm)	1	3
Temperature (°C)	700–1000	650–850
Anode	Nickel/zirconia	Nickel
Cathode	Lanthanum manganite	Nickel oxide
Interconnect	Lanthanum chromite	Stainless steel
Maximum power (kW)	25	100
Maximum life (h)	50 000	10 000
Efficiency (%)	50–60	45–50
Problems	Leaks, thermal shocks	Corrosion

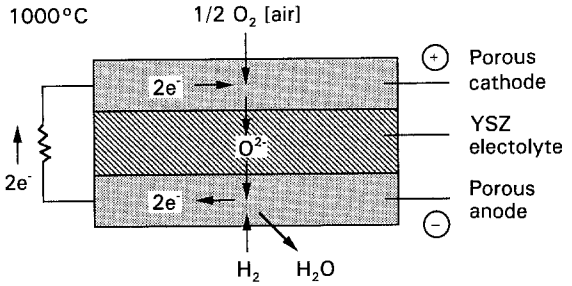

Cathode: $1/2\ O_2 + 2e^- \rightarrow O^{2-}$

Anode: $H_2 + O^{2-} \rightarrow H_2O + 2e^-$

Cell: $H_2 + 1/2\ O_2 \rightarrow H_2O$

$(CO + 1/2\ O_2 \rightarrow CO_2)$

Figure 1 Electrode reactions in a solid oxide fuel cell.

the SOFC over the MCFC is that there is a problem of electrolyte migration in the latter, while no such problem exists in the former [6]. Furthermore, the kinetics of the present-day SOFCs are faster than their molten carbonate counterparts. The electrode reactions in a typical SOFC are schematically represented in Fig. 1.

The material hitherto used as the solid electrolyte in most of the experimental fuel cells is yttria-stabilized zirconia (YSZ), because of its higher conductivity and desirable stability in both oxidizing and reducing atmospheres. The electrolytic and material properties of stabilized zirconia have been extensively studied and a number of excellent reviews on the subject are available [9–14]. Stabilized zirconia, however, requires an operation temperature of $\sim 1000\,^{\circ}C$ due to conductivity requirements. Various problems are associated with such a high temperature: thermal stresses at the electrolyte–electrode and electrode–interconnect interfaces, interdiffusion between electrodes and electrolyte and degradation of the electrodes due to demixing. A substantial effort has been made to develop electrolytes, alternative to stabilized zirconia, with higher ionic conductivity at lower temperatures. Lowering the temperature would also extend the operating life of fuel cells and ensure a shorter heating time before the start-up. With this aspect in view, quest for the development of new electrolytes has been revitalized.

Several studies [15–25] have shown that ceria (CeO_2) doped with alkaline-earth or rare-earth oxides exhibits ionic conductivity up to two orders of magnitude higher than zirconia at comparable temperatures. Ceria has the same fluorite structure as thoria and doped zirconia, but is different in that pure CeO_2 undergoes large departures from stoichiometry at elevated temperatures, leading to appreciable electronic conduction, which is undesirable. Yahiro *et al.* [26] overcame this problem by coating the CeO_2-based electrolyte with a film ($\sim 1\ \mu m$) of YSZ. The resulting "composite solid electrolyte" exhibited high ionic transport number, an output voltage close to the theoretical value, and higher conductivity than a single-phase YSZ in the range 600–800 °C.

Metastable tetragonal zirconia polycrystals (TZP) have been shown to exhibit ionic conductivity higher than YSZ below 400 °C and are poor electronic conductors [27–29]. Yttria-doped tetragonal zirconia has been tested as a component of a composite electrolyte with 20 wt % Al_2O_3 [30, 31]. Addition of the insulating phase has been found to enhance the conductivity. Alumina is believed to act as a scavenger of the glassy phase that is usually encountered at the grain boundaries in pure TZP; this glassy phase hinders the transport of ions at the grain boundaries. Tetragonal CeO_2–ZrO_2 ceramics, though they may suffer from partial electronic conduction in reducing atmospheres, possess good fracture strength and fracture toughness [32–34].

A replacement of YSZ by an intermediate-temperature oxide ion conductor in SOFCs would mean significant reduction in the material and fabrication problems and improvement in the cell reliability during prolonged operation. In this connection, several doped-perovskite solid electrolytes such as $DyAlO_3$, $CaAl_{0.7}Ti_{0.3}O_3$, $BaTb_{0.9}\ In_{0.1}O_3$, $BaCe_{0.9}\ Gd_{0.1}O_3$, $BaTh_{0.9}Gd_{0.1}O_3$, and $SrZr_{0.9}Sc_{0.1}O_3$, etc., have been identified [35–37]. However, several of these materials (most of which are protonic conductors) do not possess long-term phase stability as manifested in unsteady operating potential as a result of ageing under intermediate-temperature fuel cell operating conditions [38].

Goodenough *et al.* [39] and Steele [40] have outlined the strategies to develop inexpensive oxide ion conducting materials, related to fluorite (or fluorite-type), perovskite (or perovskite-type), brownmillerite and pyrochlore structures that promise acceptable performance at temperatures in the range 400–800 °C. Some of the compounds related to brownmillerite, which have been envisaged to be new solid electrolytes are $Ba_2In_2O_5$ [39], $Ca_2Cr_2O_5$ [41] and $Ba_2GdIn_{1-x}Ga_xO_5$ ($x = 0$, 0.2, 0.4) [42]. Despite the discovery of newer electrolytic materials, it should be pointed out

that other relevant properties such as the electrolytic domains, mechanical and thermal stability, coefficient of thermal expansion, etc., are needed to be thoroughly investigated and optimized before these novel materials can become economically viable alternatives to the well-established stabilized zirconia-based electrolytes in fuel cell applications.

In cells where hydrogen is likely to be used as the fuel, protonic conductors instead of oxide electrolytes could as well be used. Iwahara *et al.* [43–45] have found that the perovskite-type oxides based on $SrCeO_3$ and $BaCeO_3$ with partial substitution of Ce^{4+} by some of the rare-earth ions (Ln^{3+}) are excellent high-temperature proton conductors. Heed and Lunden [46] had demonstrated that a fuel cell could be operated with a solid sulphate (such as lithium sulphate) electrolyte. Recently, Lunden *et al.* [47] have examined the performance of lithium sulphate in a fuel cell using hydrogen and town gas as the fuel.

Yet another promising material is stabilized bismuth sesquioxide on which scientific literature still continues to grow. Stabilized bismuth oxide (Bi_2O_3) exhibits the highest ionic conductivity at comparable temperatures. This greater ionic conductivity of stabilized Bi_2O_3 offers the possibility of its use as an electrolyte in SOFCs operated at lower temperatures ($< 1000\,°C$). It is the purpose of this paper to review some of the developments in the area of bismuth sesquioxide-based solid electrolytes.

2. Bismuth sesquioxide-based electrolytes for fuel cells

Pure bismuth sesquioxide has two thermodynamically stable crystallographic polymorphs [48–54]. One is α-Bi_2O_3, which is stable below 730 °C and has a monoclinic structure, which shows p-type conduction [55]. The other is δ-Bi_2O_3, which is stable above 730 °C, up to its melting temperature of 825 °C, and crystallizes in the fluorite (cubic, CaF_2) structure. In addition to these phases, tetragonal (β-Bi_2O_3) and body-centred cubic (γ-Bi_2O_3) crystallographic modifications are also known to exist below 650 °C, as metastable phases.

The CaF_2-type δ-Bi_2O_3 contains 25% of the anion sites (one oxygen site per formula) vacant, and as a result exhibits very high O^{2-} ion conductivity ($\sim 1\,\Omega^{-1}\,cm^{-1}$ near the melting point). The conductivity is up to two orders of magnitude greater than that in the stabilized zirconia. The high polarizability of the Bi^{3+} ion with its lone pair of electrons has been viewed as a conductivity-enhancing factor [56]. Another possibility could be the existence of a weaker metal–oxygen bond between bismuth and oxygen as compared to that between zirconium and oxygen; this might promote a greater mobility of the vacancies in the lattice.

However, the high conductivity phase is stable over a very narrow range of temperature (730–825 °C). Further, the volume change associated with the $\delta \rightarrow \alpha$ transition leads to cracking and severe deterioration of the material. Thus, for application of Bi_2O_3 as a solid electrolyte in fuel cells, it is imperative that the high-temperature cubic phase be stabilized. The temperature dependence of conductivity of various solid oxide electrolytes is shown in Fig. 2. It is clear that the Bi_2O_3-based materials stand out as superior oxide electrolytes. However, the main drawback of this material is its small oxygen potential range of ionic conduction (electrolytic domain). Stabilized Bi_2O_3 is prone to reduction into metallic bismuth, even at moderately low oxygen partial pressure.

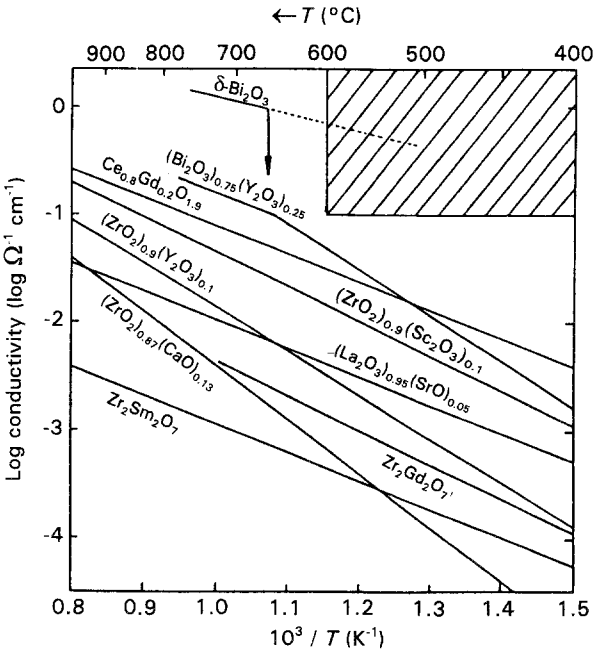

Figure 2 Temperature dependence of oxide ion conductivity in selected ceramic oxides [31].

A large number of studies has shown that the high conductivity δ-phase in Bi_2O_3 could be stabilized at lower temperatures, by the addition of dopants (see the subsequent sections). However, doping (by various di-, tri-, tetra-, penta- or hexavalent cations) also lowers the ionic conductivity. In some cases, doping leads to transformation into a more conducting rhombohedral phase which, however, undergoes decomposition with a concurrent decrease in the ionic conductivity at temperatures below 700 °C [57, 58]. The extent and nature of the phase structure of the doped Bi_2O_3 (i.e. f c c or rhombohedral or a mixture of both), depends on the ionic radii of the dopants, their proportion (mole fraction) in the host material and thermal history. Recent work by Fung and Virkar [58] has shown that stabilization of the high-conductivity phase in doped Bi_2O_3 can further be achieved by adding a second dopant such as calcia, strontia, zirconia or thoria. However, like ceria-based electrolytes, the low decomposition oxygen potential of Bi_2O_3 precludes its direct contact with the fuel and, in real applications, the fuel-side surface of the electrolyte should be coated with a thin layer of more stable electrolyte, such as YSZ. This would prevent the reduction of the electrolyte, while the overall internal resistance (and hence the iR drop, where i is the current and R the resistance) can be substantially lower compared to an all-zirconia electrolyte.

Recently, Virkar [59] has pointed out that the logic behind depositing a thin YSZ layer could be an oversimplification, as the coating does not necessarily ensure the stability of the electrolyte itself. Whether the electrolyte is or is not stable, will depend mainly on the oxygen chemical potential that would exist at the interface between the protective layer and the electrolyte. The oxygen potential, in turn, depends upon a number of operational parameters of the fuel cell, of which the most important is the conduction characteristics of the two-layer composite electrolyte. The interfacial oxygen chemical potential and thus the stability of the electrolyte and of the SOFC has been shown [59] to depend critically on the transport characteristics of the interface. Cathodic potentials of -0.64 V ($p_{O_2} \simeq 10^{-13}$ atm) at 600 °C are sufficient to produce rapid degradation of stabilized Bi_2O_3 electrolytes [60]. Thus from a practical point of view, the use of stabilized Bi_2O_3 as an alternate SOFC electrolyte is questionable, unless techniques are developed to protect the electrolyte from direct exposure to such low P_{O_2} environments, by means of compositing or thin-film deposition with more stable material with comparable ionic conductivity. In other words, for viable applications, the thermodynamic stability of the proposed electrolyte in reducing atmospheres as well as phase stability at lower temperatures must be enhanced.

In the following sections, various investigations pertaining to the stabilization of δ-Bi_2O_3 through doping are reviewed. For simplicity and clarity, the discussion is divided according to the charge of the dopant cations.

2.1. Bi_2O_3–MO (M = Ca, Sr, Ba) system

Levin and Roth [61], Takahashi *et al.* [62] and Conflant *et al.* [63] studied the phase equilibria in these pseudobinaries. Takahashi *et al.* also studied the electrical characteristics of the Bi_2O_3–CaO solid solutions. Conflant *et al.* could delineate this system in terms of four incongruently melting compounds ($Bi_{14}Ca_5O_{26}$, Bi_2CaO_4, $Bi_{10}Ca_7O_{22}$ and $Bi_6Ca_7O_{16}$) and four solid solutions (fcc, bcc and two rhombohedral). They also observed that the rhombohedral solid solution in calcia-stabilized Bi_2O_3 was isostructural with Bi_2O_3–CdO, investigated earlier by Sillen and Sillen [64]. Takahashi *et al.* [62] found that the rhombohedral phase showed high oxygen ion conductivity.

The X-ray diffraction studies of Sillen and Aurivillius [65] showed that SrO has a wide range of solid solutions with Bi_2O_3, beginning at 14 mol % SrO. The solid solution was ascribed a rhombohedral lattice structure, with vacancies in the anion sublattice, which was later confirmed by Levin and Roth [61], Takahashi *et al.* [62] and Conflant *et al.* [66]. Neuimin *et al.* [67] investigated the electrical conductivity of solid solutions of Bi_2O_3 with 15–20 mol % SrO in the range 400–600 °C. The electrical conductivity in the isostructural solid solution Bi_2O_3–CdO was studied by Hauffe and Peters [68], who observed that the conductivity was a strong function of the partial pressure

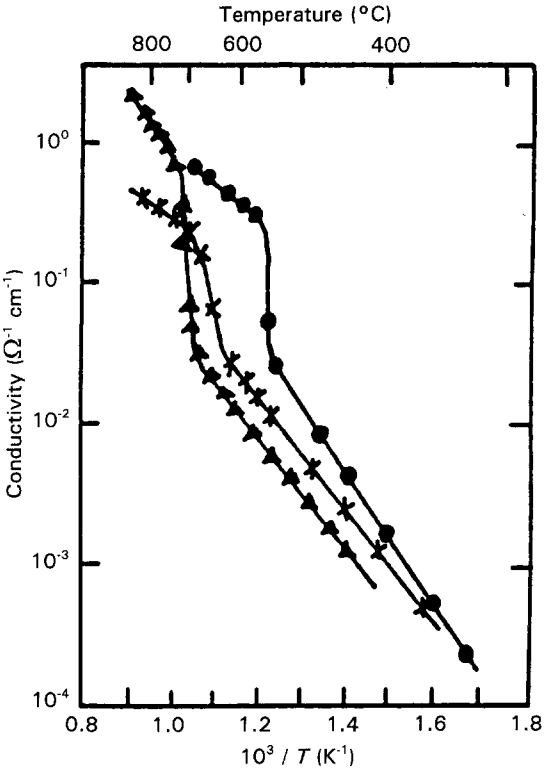

Figure 3 Conductivity of rhombohedral phase in alkaline earth-stabilized Bi_2O_3 solid solutions $(Bi_2O_3)_{0.8}(MO)_{0.2}$: (▲) Ca; (×) Sr; (●) Ba [85].

of oxygen in the gas phase. Therefore, despite the presence of a large number of oxygen ion vacancies in the crystal lattice, the conductivity was predominantly electronic. The experimental results of Neuimin *et al.* [67] with Bi_2O_3–SrO solid solutions as the electrolyte in fuel cells indicated that in an atmosphere with a relatively high oxygen partial pressure (oxygen versus air), these phases had a considerable fraction of ionic conductivity, which increased with an increase in temperature. On the other hand, when air at the anode was replaced with a fuel mixture of 66% CO and 34% CO_2, the e.m.f. indicated the presence of electronic conductivity in the electrolyte (0.8 Bi_2O_3 + 0.2 SrO), which increased with an increase in temperature. In another set of experiments, they investigated the following fuel cell in the temperature range 500–650 °C

$$\text{NiO, air}/0.85\ Bi_2O_3 + 0.15\ \text{SrO}/\text{CO, Ni}$$

The i–V (V is the voltage) characteristics of these cells indicated that while there was little polarization of the electrodes at 600 and 650 °C, it was significant at 500 °C. Short-circuit currents were also found to be unsteady with time in the case of both these electrolytes. Post-experiment examination of the solid electrolyte made of 0.8 Bi_2O_3 + 0.2 SrO and 0.85 Bi_2O_3 + 0.15 SrO showed air holes and fused metallic globules (bismuth) on the fuel side, indicating reduction of Bi_2O_3 by the fuel gas.

The fact that the conductivity in the rhombohedral phase containing SrO was somewhat higher than that in the CaO analogue was explained by Takahashi *et al.* [62] in terms of the cation size effect (the radius of Sr^{2+} is larger than that of Ca^{2+}). Moreover, it led

to the speculation that the rhombohedral phase in the baria-doped bismuth oxide could possess even higher conductivity. Substitution of Bi^{3+} ions by the alkaine-earth metal ions of increasing size is likely to favour atomic rearrangements, leading to a transition from the more ordered fcc to the relatively less ordered rhombohedral structure. From this point of view, the electrical conductivity measurements in the solid solutions of Bi_2O_3–BaO pseudo-binary in the range 10–67 mol % and 12–32 mol % BaO, were conducted by Takahashi *et al.* [62, 69] and Suzuki *et al.* [70], respectively. The variation of conductivity with temperature for CaO-, SrO- and BaO-doped bismuth oxide is shown in Fig. 3. A common feature of these plots is the abrupt jump in the conductivity at $\sim 600\,^{\circ}C$. This was attributed to the $\beta_1 \rightarrow \beta_2$ transition within the rhombohedral structure. It could also be seen that among the three alkaline-earth oxide dopants, BaO has the most benign effect in that it has the lowest transition temperature and the conductivity of the high-temperature modification, β_1, is $0.01\ \Omega^{-1}\,cm^{-1}$ at 500 °C (20 mol % BaO [69]) and $0.88\ \Omega^{-1}\,cm^{-1}$ at around 600 °C (16 mol % BaO [70]): one of the highest among the Bi_2O_3-based oxides. An interesting observation made by Suzuki *et al.* [70], was that the grain orientation and conductivity of the slowly cooled samples were better than those of the quenched ones.

The effect of doping by alkaline-earth metal ions can be very well appreciated by knowing the component thermodynamic activities in the corresponding solid solutions. For example, there are several intermediate stoichiometric compounds in the MO–Bi_2O_3 systems. On the basis of solution thermodynamics, compound formation indicates a lowering of activity of a given component. In other words, it is a measure of negative deviation of thermodynamic activity from ideality. Thus, in such systems, there would be compositions which would exhibit activity coefficient ($\gamma = a_{MO}/x_{MO}$) less than unity, and hence better thermodynamic stability in a reducing atmosphere (a_{MO} is the activity of MO). Baek and Virkar [71] recently used solid fluoride electrolyte-based galvanic cells for the determination of activity-composition relations in the MO–Bi_2O_3 systems, employing the following typical cell configuration

$$Ag/air, MF_2, (Bi_2O_3)_{1-x}(MO)_x/ \qquad MF_2/MF_2,MO, air/Ag$$

The compositions studied were $0.26 \leqslant x \leqslant 0.31$ for the CaO–Bi_2O_3 system; $0.23 \leqslant x \leqslant 0.43$ for the SrO–Bi_2O_3 system and $0.26 \leqslant x \leqslant 0.33$ for the BaO–Bi_2O_3 system. The directly measured activity of MO, a_{MO}, in these solid solutions is given by the Nernst equation

$$a_{MO} = \exp(-2FE/RT) \qquad (1)$$

where F is the Faraday constant and E represents the electromotive force of the galvanic cell. R and T have their usual meanings. From the measured activities of MO, those of Bi_2O_3 in these solid solutions have been derived, as a function of compositions, with the help of Gibbs–Duhem integration. The activity of Bi_2O_3 for the richest MO compositions at 630 °C were reported to be 0.56 in CaO–Bi_2O_3 ($x_{CaO} = 0.31$), 0.12 in SrO–Bi_2O_3 ($x_{SrO} = 0.43$) and 0.56 in BaO–Bi_2O_3 ($x_{BaO} = 0.33$). The activity of Bi_2O_3 is the lowest (0.12) in the SrO–Bi_2O_3 system. Accordingly the rhombohedral phase in the strontia-doped bismuth oxide system with the highest dopant concentration would be the most stable phase in reducing atmosphere. At 670 °C, the lowest oxygen partial pressures for which pure Bi_2O_3 and $(SrO)_{0.43}(Bi_2O_3)_{0.57}$ are stable are 3×10^{-12} and 6×10^{-13} atm, respectively. Thus from the standpoint of thermodynamic stability, the alkaline-earth oxide-stabilized Bi_2O_3 is preferable to pure Bi_2O_3, with the SrO-stabilized rhombohedral phase ($x_{SrO} = 0.43$) being the most stable [72].

2.2. Bi_2O_3–RE_2O_3 (RE = Y and/or rare-earth metal) system

The ceramic alloys of bismuth oxide containing rare-earth cations have been most extensively investigated, both from the viewpoint of establishing accurate phase relationships and to explore their conduction characteristics. One of the most interesting features of the rare-earth stabilization of Bi_2O_3 is that unlike in the case of alkaline earth–Bi_2O_3 system, for which the high conductivity phase is rhombohedral, the cubic (fcc) phase is more conducting and can be retained at lower temperatures ($\sim 400\,^{\circ}C$) for longer periods by addition of second dopants. This aspect of phase stability has a direct bearing on the long-term application of these phases in fuel cells over a large number of thermal cycles. Of these, the Y_2O_3–Bi_2O_3 system has been studied in most detail.

2.2.1. Stabilization with one rare-earth oxide

2.2.1.1. Bi_2O_3–Y_2O_3 system. The electrical and thermal properties of the δ-phase stabilized by Y_2O_3 have been measured by several investigators [73–82]. Levin and Roth [83] and Datta and Meehan [84] investigated the Y_2O_3–Bi_2O_3 phase diagram. These workers indicate that the δ-phase in samples containing 25 mol % Y_2O_3–75 mol % Bi_2O_3 is stable below 400 °C. Takahashi and Iwahara [85] suggested that this composition might be the most desirable one for practical use of this electrolyte as an oxide ion conductor in fuel cells. According to their study, this composition had the lowest yttria content at which no transformation occurred and had the highest conductivity over a wide range of temperature. The phase equilibrium study of Datta and Meehan [83] showed that the δ-phase, forming a limited solid solution could be stabilized thermodynamically towards room temperature. However, based on their study in the limited composition range (21.5–23.5 mol % yttria), Watanabe and Kikuchi [80] and recently, Watanabe [86] showed the existence of a new low-temperature stable phase having hexagonal (or rhombohedral) symmetry in the same composition range. They reported that this low-temperature stable hexagonal phase transforms reversibly around 720 °C into the high-temperature, oxygen-deficient fluorite-type structure. Several

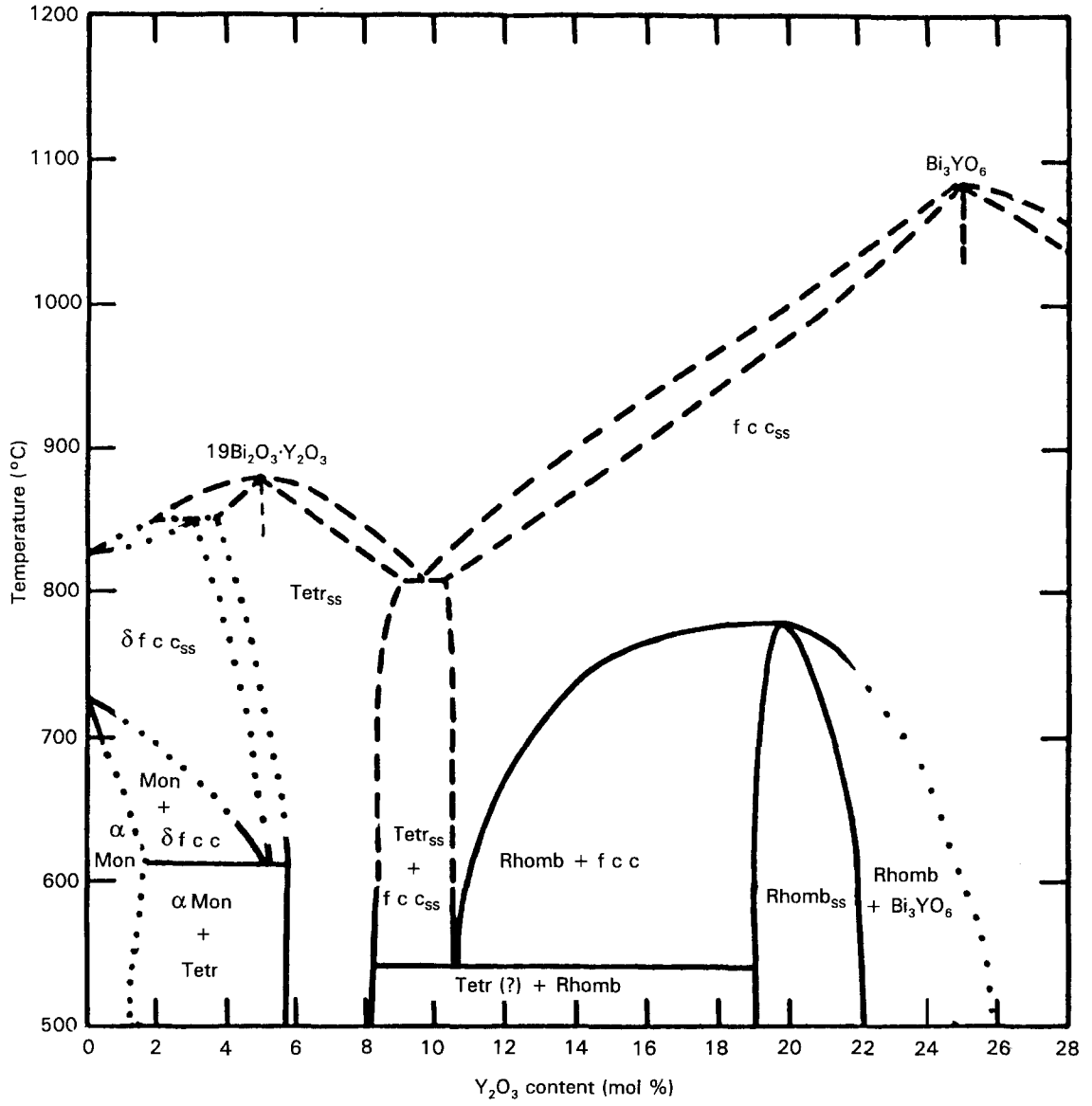

Figure 4 Revised phase diagram for the system Bi_2O_3–Y_2O_3. (– – –) Datta and Meehan [84], (——) Powers [88].

subsequent phase equilibrium studies have indicated this diagram to be incorrect. For instance, the diagram clearly leaves the region between 0 and 2 wt % Y_2O_3 uncertain. On the basis of an argument based on the relation between the size of the dopant cation and the general shape of the Bi_2O_3-rich portion of the phase diagram, Powers concluded that the diagram of Datta and Meehan is incorrect [87, 88]. Moreover, the presence of a wide range of solid solution for tetragonal phase and the absence of any rhombohedral phase in the Bi_2O_3-rich region in their phase diagram has also been refuted in the literature. Joshi *et al.* [79] observed that in the work of Datta and Meehan, the use of ultra-high-purity materials might be the principal factor which prevented the establishment of equilibrium conditions and led to erroneous phase relationship. They pointed out that if the two component oxides are very pure, so will be the resultant solid solution. This means that very few point defects would be available for mass transport. Thus in the solid solution, "near intrinsic" conditions might have prevailed, thereby rendering the kinetics of mass transport very sluggish.

Powers [88] redetermined the Bi_2O_3–Y_2O_3 phase diagram by high-temperature X-ray diffraction (XRD) and differential thermal analysis (DTA) techniques (Fig. 4). For comparison, Datta and Meehan's results are also shown in the same figure by broken lines. According to this diagram, at ~ 725 °C or lower, the cubic solid solution would decompose. Kruidhof *et al.* [81] recently investigated the thermochemical stability of yttria-stabilized Bi_2O_3 solid solutions, containing 22–32.5 mol % Y_2O_3. They reported that the solid solutions containing less than 31.8 mol % Y_2O_3 were cubic (f c c), and were metastable at temperatures below ~ 840 °C. During annealing at 650 °C, a sluggish transformation (cubic → hexagonal) occurs. The hexagonal phase is transformed rapidly into the cubic phase above 740 °C. These observations are in conformity with those of Powers [88].

The conductivities of the sintered Bi_2O_3–Y_2O_3 solid solutions (in the range 0–60 mol % Y_2O_3) in air,

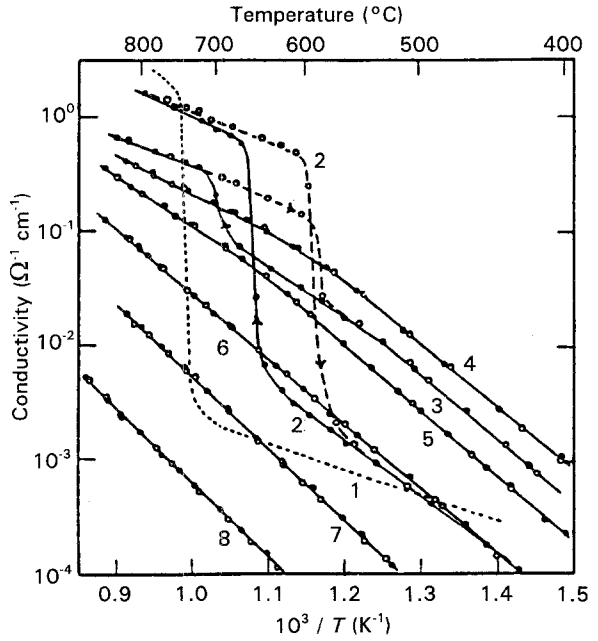

Figure 5 Conductivity of $(Bi_2O_3)_{1-x}(Y_2O_3)_x$ in air [71]: the numbers represent the mole fraction (x) of Y_2O_3 in the solid solutions, 1: 0.0; 2: 0.05; 3: 0.20; 4: 0.25; 5: 0.33; 6: 0.425; 7: 0.50; 8: 0.60.

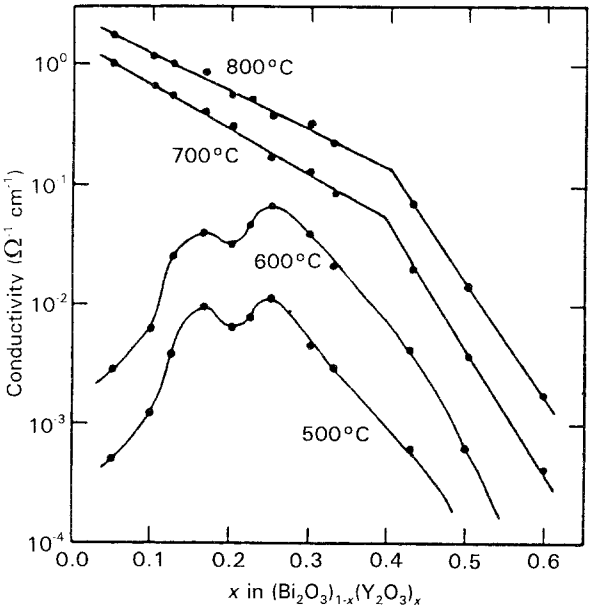

Figure 6 Oxide-ion conductivity isotherms of $(Bi_2O_3)_{1-x}(Y_2O_3)_x$ in air as a function of composition [74].

reported by Takahashi *et al.* [74] are shown in Fig. 5. Some interesting observations could be made from this figure. First, the conductivity of pure Bi_2O_3 is relatively low below 730 °C; above this temperature the phase transformation from monoclinic to cubic is attended by a sudden increase (jump) in conductivity [89, 90]. Second, the conductivity of sintered samples containing less than 25 mol % Y_2O_3 showed significant hysteresis. For example, the temperatures at which such samples (curves 2 and 3 in Fig. 5) showed a jump in conductivity, differed by ~ 50–100 °C in the heating and cooling cycles. Third, the magnitude of the jump in conductivity decreased, and eventually disappeared as the amount of yttria in the sintered samples increased (curves 3–8). In these cases, the discontinuity (observed clearly for 25 mol % Y_2O_3 samples) was ascribed to a second-order phase transition in the stabilized δ-phase. Takahashi *et al.* [74, 85], however, did not identify the exact phase relation, nor did they report any crystallographic data for the other phase. As pointed out earlier, Watanabe and Kikuchi [80] and later Watanabe [86] identified the low-temperature stable phase for the composition 25 mol % Y_2O_3 to be hexagonal. Their d.c. conductivity results for the hexagonal and cubic phases, having the composition $(Bi_2O_3)_{0.775}$–$(Y_2O_3)_{0.225}$ show that the conductivity of the hexagonal phase is about an order of magnitude lower than that of the metastable phase.

The dopant concentration versus conductivity isotherms, determined by Takahashi *et al.* [74] are shown in Fig. 6. In the temperature range of 700 °C and above, where the fcc single phase is stable, the conductivity decreases monotonically with increasing dopant concentration. The change in the slope at ~ 40 mol % Y_2O_3 has been ascribed to the saturation solubility limit of Y_2O_3 in the fcc phase. At lower temperatures, the conductivity exhibits two maxima: one at ~ 17 mol % Y_2O_3 and the other at ~ 25 mol % Y_2O_3. The conductivity of the 25 mol % Y_2O_3–Bi_2O_3 solid solution is higher than that of 17 mol % Y_2O_3–Bi_2O_3 solid solution. The conductivity is seen to decrease rather sharply on either side of these two maxima. While the maximum in conductivity at 25 mol % Y_2O_3 has been explained to be due to the composition being on the lower end of the solubility limit of yttria in the fcc phase at these temperatures, that at < 17 mol % yttria has not been explained yet. The occurrence of a conductivity maximum at a certain composition of the dopant, is similar to the general trend for stabilized zirconias, where the composition possessing the highest oxide ion conductivity lies at the lowest content of the second cation within the range of a single-phase solid solution formation. The investigation of the solid solution $(Bi_2O_3)_{1-x}$–$(Y_2O_3)_x$ in the range of $x = 0.17$–0.25 at temperatures up to 700 °C and the exploration of the origin of the dip in the conductivity versus composition curves may lead to ways to suppress and/or eliminate it. The decrease in conductivity beyond the second maximum is suggestive of significant interaction energy between the oxide ion vacancy and the dopant cation (and not due to that among the oxide ion vacancies) [85].

As will be seen later in this paper, the destabilization of high-conductivity cubic phase into a low-conductivity rhombohedral phase over some composition range appears to be a general feature of the rare-earth oxide–bismuth oxide systems, and the high conductivity cubic phase may, in fact, be a metastable one below ~ 700 °C. This is a serious shortcoming of the stabilized bismuth oxide electrolytes in that many of these "high conductivity" compositions may be of little practical use for applications involving isothermal operations below ~ 700 °C for periods of the order of several hundred hours or more. In order to enhance the stability of the cubic phase at lower temperatures,

Fung and Virkar [58] have suggested the use of CaO, Sro, ZrO_2 and ThO_2 as the aliovalent stabilizing dopant in the 25 mol % Y_2O_3–75 mol % Bi_2O_3 solid solutions.

Contrary to the observation by Takahashi *et al.* [60] and Verkerk and Burggraaf [91], that an oxygen partial pressure of the order of 10^{-12}–10^{-13} atm would result in the reduction of bismuth oxide to metallic bismuth, Wang *et al.* [78] and, subsequently, Duran *et al.* [92] and Jurado *et al.* [93] reported ionic conductivity in the stabilized Bi_2O_3 over an extended range of oxygen partial pressure (up to 10^{-21} atm) at 700 °C. This discrepancy calls for the re-examination of the thermodynamic stability of the pure and the doped bismuth oxides by the solid-state galvanic cell technique, vapour pressure measurements and calorimetric methods.

2.2.1.2. Bi_2O_3–La_2O_3 system. Takahashi *et al.* [62] first investigated the ionic conduction characteristics of sintered oxide solid solutions of Bi_2O_3 containing 10–30 mol % La_2O_3. The E/E_0 values (representing oxide ion transport number), measured by a standard concentration cell ($p_{O_2} = 1.0$ atm versus $p_{O_2} = 0.21$ atm) employing the lanthanum oxide-doped Bi_2O_3, were found to be greater than 0.9 (0.92–0.95) in the temperature range 550–750 °C. However, the electrolytes in this system are prone to reduction in lower oxygen partial pressure domains, where electronic conduction would dominate. The phase relationships in the Bi_2O_3–La_2O_3 and the Bi_2O_3–La_2O_3–TeO_2 system were studied by Watanabe [86] and Mercurio *et al.* [94], respectively. As mentioned earlier, Watanabe identified a hexagonal (rhombohedral) layered structure as the low-temperature stable modification, which showed good oxide-ion conductivity. However, these structures are prone to gradual decomposition in humid environments even at room temperatures [95]. Mercurio *et al.* [94], who studied the pseudo-ternary system over a wide range of rare-earth oxide and TeO_2 composition, identified as many as five solid solutions labelled Q (tetragonal), F, F′ (cubic), and ε and R (rhombohedral) in the Bi_2O_3–La_2O_3–TeO_2 system. It has been shown that the electrical characteristics within different domains of these solid solutions are essentially dependent on (i) the nature of rare-earth cation (Ln^{3+}), (ii) the amount of rare-earth oxide dopant, (iii) the amount of TeO_2 and (iv) the structure of the solid solution.

The best electrical properties were shown to be possessed by the anion-deficient fluorite-like F and F′ phases; the conductivity was highest for the phase $(Bi_2O_3)_{0.90}(La_2O_3)_{0.06}(TeO_2)_{0.04}$. At 350 °C, the conductivity was 0.0050 $\Omega^{-1}\,cm^{-1}$. In the molar concentration range higher than 10% for the rare-earth oxide, the conductivity decreased as the La_2O_3 content increased. The conductivity also decreased with increase in TeO_2 content. This is possibly due to the decrease in the oxygen ion vacancy concentration. The higher conductivity exhibited by the rhombohedral phase, in comparison to the fcc phase, at temperatures lower than 200 °C has been ascribed to the lower activation energy of migration of oxygen ions in that phase. However, the oxygen potential in TeO_2 is lower than even that in the host Bi_2O_3, and hence exposure of solid electrolyte based on this system even to a relatively moderate oxygen partial pressure may tend to reduce the Te^{4+} cations. This reduction may eventually result in the degradation of the electrolytic properties of these materials.

2.2.1.3. Bi_2O_3–Gd_2O_3 system. Datta and Meehan [84] studied the phase diagram of the pseudobinary Bi_2O_3–Gd_2O_3 system, while Takahashi *et al.* [96] investigated the phase relationships as well as the electrical conductivity in the sintered bodies of Bi_2O_3–Gd_2O_3 solid solutions, with gadolinia content ranging from 5–50 mol %. In contrast to the observation of a single fcc phase by Datta and Meehan in the composition range 10–50 mol % Gd_2O_3 over a wide temperature range, Takahashi *et al.* showed that in the 5–30 mol % Gd_2O_3 range, the high-temperature fcc phase is unstable at low temperatures. The solid solutions containing 5–10 mol % Gd_2O_3 transformed into tetragonal and those containing 10–30 mol % Gd_2O_3, into rhombohedral phase, as the temperature was lowered.

The conductivity curves of the sintered Bi_2O_3–Gd_2O_3 solid solutions were qualitatively similar to those observed by the same authors in Bi_2O_3–Y_2O_3 solid solutions [74]. For samples containing less than 35 mol % Gd_2O_3, the conductivity showed an abrupt rise corresponding to the phase transformation from tetragonal (or rhombohedral) to cubic. It may be noted that the temperature at which conductivity showed a jump shifted to values less than 730 °C (for monoclinic to cubic in pure Bi_2O_3) for compositions up to 10 mol % Gd_2O_3, but to higher than 730 °C for samples containing gadolinia in the range $0.10 < x < 0.35$. These temperatures are considered to be the transition temperatures from tetragonal to fcc in the first case and from rhombohedral to fcc in the second. For the Gd_2O_3-rich ($x > 0.35$) compositions, the single linear correlation between $\log \sigma - 1/T$, where σ is the conductivity, is suggestive of the existence of a single fcc phase from room temperature up to ~ 900 °C.

The conductivity of these solid solutions measured in the range 1–10^{-5} atm oxygen partial pressure, indicated that the conduction was purely ionic and due only to oxide ions over the temperature range 600–800 °C. Moreover, the conductivity was found to be independent of the phase transformation. In terms of magnitude, these conductivities were comparable to those in the Bi_2O_3–Y_2O_3 system. At 600 °C, the conductivities of the rhombohedral $(Bi_2O_3)_{0.9}(Gd_2O_3)_{0.1}$ and the fcc $(Bi_2O_3)_{0.65}(Gd_2O_3)_{0.35}$ are 0.045 and 0.024 $\Omega^{-1}\,cm^{-1}$, respectively: about an order of magnitude higher than those in YSZ at the corresponding temperature.

Recently, Su and Virkar [97] investigated the ionic conductivity by the a.c. impedance technique, and the kinetics and sequence of phase transformation in $(Bi_2O_3)_{0.86}(Gd_2O_3)_{0.14}$ by microstructural analyses

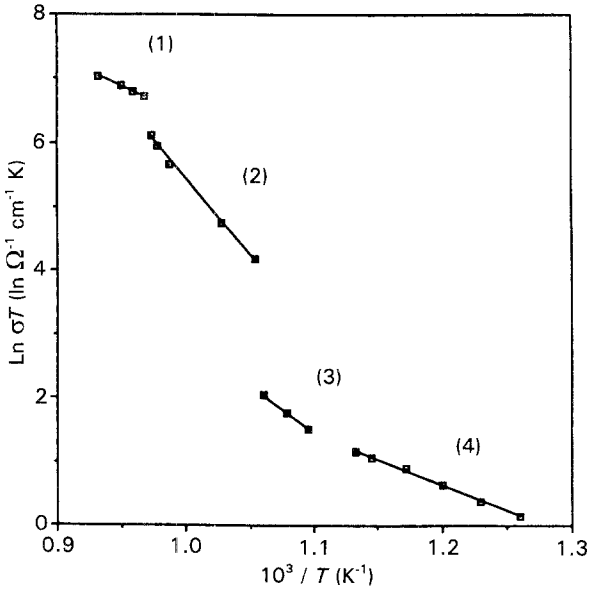

Figure 7 Conductivity of equilibrated samples of $(Bi_2O_3)_{0.86}(Gd_2O_3)_{0.14}$, showing Arrhenius behaviour [97]. Regions 1 and 4 correspond to single-phase cubic and rhombohedral solid solutions; regions 2 and 3 correspond to two-phase mixtures: 2. rich in cubic and 3 rich in rhombohedral phase.

using XRD and transmission optical microscopy, both as a function of temperature and time. The choice of this composition was based on the observation that at high temperatures this composition corresponds to a single-phase f c c material, while at low temperatures it corresponds to a single-phase rhombohedral material, as noted by Takahashi *et al.* [96]. It was observed that above 760 °C, the samples are fully cubic and below 610 °C they are entirely rhombohedral. In the temperature range between these two extremes the equilibrium state corresponds to the two-phase field containing the cubic and the rhombohedral phases. In accordance with these microstructural and phase analyses findings, there were four distinct regions in the measured log σ versus $1/T$ plots (Fig. 7); two single-phase and two two-phase regions. One of these two-phase regions corresponds to a regime where the high-conductivity cubic phase is contiguous. The equivalent circuit model suggests the conduction behaviour to follow a parallel path in this region. The other region, which occurs at lower temperatures, has been envisaged as that containing the high conductivity phase in isolated pockets. In this regime the equivalent circuit model for the requisite conduction conforms to that for series paths. This investigation is an important contribution to the understanding of conduction behaviour of stabilized bismuth oxide systems in terms of the evolution of different phases and their conduction characteristics, as a function of time and temperature. These observations also emphasize the need to study the implications of the transformation from the rhombohedral to the cubic phase and vice versa in real fuel cell applications.

2.2.1.4. Bi_2O_3–Dy_2O_3 system. Verkerk and Burggraaf [98] investigated the phase diagram and oxygen ion conductivity in this system, in the composition range 5–60 mol % Dy_2O_3. The samples containing 5 mol % Dy_2O_3 had a tetragonal structure up to 640 °C above which it transformed into the high-temperature cubic (f c c) phase. Annealing for ~ 350 h at 550 °C resulted in some minor phases, in addition to the main tetragonal structure. The samples containing 10–25 mol % Dy_2O_3 were mainly cubic at high temperatures, as deduced from quenching experiments, whereas the low-temperature modification was rhombohedral from about 15–25 mol % dysprosia. The equilibrium monophase cubic structure was stable at low temperatures for the solid solutions containing 28.5–50 mol % Dy_2O_3. This result contradicts the observation of Datta and Meehan [84] who reported the existence of the f c c phase for the composition $(Bi_2O_3)_{0.75}(Dy_2O_3)_{0.25}$ at low temperatures. However, as noted above in the case of the solid solutions of Bi_2O_3 with yttria, this error is probably due to the non-attainment of equilibrium conditions in the experiments of Datta and Meehan. On the other hand, the investigations of Verkerk and Burggraaf confirmed the observation of the f c c phase in the solid solution $(Bi_2O_3)_{0.50}(Dy_2O_3)_{0.50}$ reported by Nasanova *et al.* [99]. Samples containing 60 mol % Dy_2O_3 showed the existence of an unknown phase together with the f c c phase. In the range 10–25 mol % dysprosia, the temperature of the rhombohedral (low-temperature) → cubic (high-temperature) phase transition showed a monotonic increase from 575 °C (for $(Bi_2O_3)_{0.90}(Dy_2O_3)_{0.10}$) to 745 °C (for $(Bi_2O_3)_{0.75}(Dy_2O_3)_{0.25}$), as deduced from DTA experiments. These results also showed one-to-one correspondence with the conductivity measurements, as shown in Fig. 8, for example, for the solid solution $(Bi_2O_3)_{0.75}(Dy_2O_3)_{0.25}$.

The discontinuity at ~ 740 ± 15 °C in the conductivity–temperature plot is attributed to the structural change from rhombohedral to f c c (~ 745 °C). The change in slope in the conductivity plot for the f c c phase at ~ 600 °C has been correlated to changes in the oxygen ordering in the cubic lattice. In the case of the cubic samples containing 25–60 mol % Dy_2O_3, the discontinuity in the conductivity versus temperature curves occurs at about 600–680 °C for the solid solutions containing 25–30 mol % Dy_2O_3; the samples containing 40–60 mol % Dy_2O_3 are cubic throughout the temperature range of measurements (300–780 °C). The highest conductivity characteristics were reported for the composition $(Bi_2O_3)_{0.715}(Dy_2O_3)_{0.285}$: $0.744\,\Omega^{-1}cm^{-1}$ at 500 °C and $15.1\,\Omega^{-1}\,cm^{-1}$ at 700 °C [98]. These values are more than an order of magnitude higher than for YSZ at the corresponding temperatures. The samples containing Dy_2O_3 in the range $0.25 \leqslant x \leqslant 0.40$, were predominantly oxygen ion conductors, while those containing 50 mol % Dy_2O_3 exhibited small partial electronic conduction and 40 Bi_2O_3–60 Dy_2O_3 solid solutions were electronic conductors. Based on a correlation between the observed conductivity and the size of Ln^{3+} ions and the concentration of the additive, Verkerk and Burggraaf envisaged that the compositions exhibiting highest oxygen conductivity with the

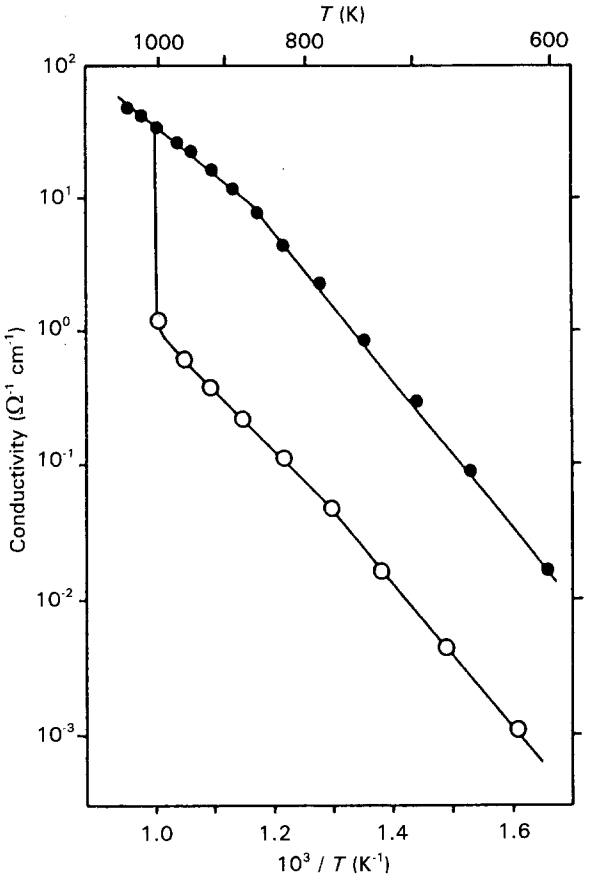

Figure 8 Conductivity of $(Bi_2O_3)_{0.75}(Dy_2O_3)_{0.25}$ in air [98]: (●) cubic; (○) rhombohedral.

lowest dopant concentration necessary to stabilize the fcc phase, would be in Er_2O_3 or Tm_2O_3-based Bi_2O_3 solid solutions.

2.2.1.5. Bi_2O_3–Er_2O_3 system. Verkerk *et al.* [100, 101] and Keizer *et al.* [102] investigated the system Bi_2O_3–Er_2O_3 over a wide range of compositions. For solid solutions containing 17.5–45.5 mol % Er_2O_3, they observed a single fcc phase, with a slight dilatation ($a \simeq 0.54$–0.55 nm) as the erbia content decreased. Below 17.5 mol % and above 45.5 mol % erbia, the solid solutions were essentially multiphase in nature. The samples could be sintered to densities near 95% theoretical at 1200 °C. In the entire temperature range of measurements (400–800 °C), the oxygen conductivity was found to be the highest in the $(Bi_2O_3)_{0.8}(Er_2O_3)_{0.2}$ solid solutions, among all the Bi_2O_3-based electrolytes as well as the zirconias. Jurado *et al.* [93] also investigated the d.c. conductivity in $(Bi_2O_3)_{0.82}(Er_2O_3)_{0.18}$ and $(Bi_2O_3)_{0.8}(Er_2O_3)_{0.2}$ cubic solid solutions. The latter composition was found to be more conductive. Kruidhof *et al.* [103] reported that the solid solutions containing up to 25 mol % Er_2O_3 show a slow transition from a cubic to hexagonal (rhombohedral) phase upon heating at 625 °C. This rhombohedral phase was stable up to 725 °C, where it re-transformed into the cubic modification. Long-term annealing at 500 °C caused the formation of traces of tetragonal Bi_2O_3, which was thought to be a result of slow decomposition of the solid solution. However, the overall structure of the solid solution was found to be cubic. In contrast to this, $(Bi_2O_3)_{0.7}(Er_2O_3)_{0.3}$ solid solutions with lower conductivity did not exhibit any of these features and hence may be better materials from the viewpoint of mechanical stability of the electrolyte.

Following the reported improvement in the electrode performance of the PbO-stabilized Bi_2O_3 electrolyte [104], Vinke *et al.* [105, 106] recently studied the oxygen transport characteristics of solid solutions containing 75 mol % Bi_2O_3–25 mol % Er_2O_3 with sputtered as well as co-pressed gold electrodes. The results showed that the electrode material, geometry and configuration had only minor influence on the rate of oxygen transfer in this electrolyte. Similar observations were earlier made by Verkerk *et al.* [101]. They studied the mechanism of oxygen transfer on stabilized zirconia-, ceria- and Bi_2O_3-based electrolytes with platinum electrodes. It was found that the electrode resistance on Bi_2O_3–Er_2O_3 was several times lower than on stabilized zirconia and ceria electrolytes. Moreover, on zirconia- and ceria-based electrolytes, diffusion of atomic oxygen on the platinum electrode was thought to be the rate-determining step in the electrode process, whereas for bismuth sesquioxide-based electrolytes, diffusion on the oxide surface was the rate-determining step. Such conclusions, however, are not substantiated by parallel investigations nor are based on firm scientific understanding of the electrode processes in these cases.

2.2.1.6. Bi_2O_3–Ho_2O_3 system. Although the ionic radii of Ho^{3+} and Y^{3+} ions are virtually the same [107], the number of studies on the solid solutions of Bi_2O_3 containing Ho_2O_3 is very small. The phase relationships in this system have been studied by Datta and Meehan [84] and Cahen *et al.* [108], who found the fcc δ-phase to have the composition $(Bi_2O_3)_{0.75}(Ho_2O_3)_{0.25}$ while in a recent study, Watanabe [109] observed hexagonal (rhombohedral) symmetry for the solid solutions containing 20.5–24.5 mol % holmia, annealed at 650 °C. These low-temperature stable hexagonal modifications were reported to have transformed into the high-temperature cubic phase upon annealing at 850 °C. The transformation was found to be quite fast in the heating mode, while the reverse (cubic to rhombohedral) was much more sluggish in the cooling direction, and therefore, the quenched fcc phase is a metastable one at lower temperatures.

Meng *et al.* [110] studied the temperature dependence of conductivity of the solid solutions containing 21.5 and 22.5 mol % Ho_2O_3. Although the conductivity of the hexagonal phase is also believed to stem from oxygen ion migration, the conductivity values reported were lower than those of the fcc phase. Watanabe ascribed this difference to the crystallographic anisotropy and polymorphic transition in the hexagonal samples. It is believed that the movement of oxygen ions is excessively blocked in the anisotropic polycrystalline sintered material (hexagonal), in

comparison with the isotropic fcc material. Investigations related to the stability and the kinetics of phase transformations in this system, and their eventual effect on the overall conductivity of the solid solutions, would be an interesting area to explore, because the conductivities in the temperature range of interest are quite significant.

As can be seen from the foregoing discussion, there is a tendency of destabilization of the cubic phase in several of the Bi_2O_3–RE_2O_3 systems. However, no systematic studies have been reported in the literature on the mechanism of destabilization, or on the suppression of the kinetics of phase destabilization. Recently, the suppression of phase transformation kinetics by the addition of 5 mol % ZrO_2 in yttria-, erbia-, gadolinia- and samaria-doped Bi_2O_3 systems has been rationalized by Fung *et al.* [72], on the premise that cation interstitials are more mobile in comparison to the cation vacancies. Incorporation of aliovalent dopants in TiO_2–SnO_2 [111–114] and $LiAl_5O_8$–$LiFe_5O_8$ [115] systems has been found to affect the kinetics of phase transformation drastically. On the basis of these observations, Fung *et al.* [72] envisaged that the dopants which enhance the interdiffusion, accelerate the transformation kinetics while those which suppress the cation interdiffusion, hinder the transformation.

2.2.2. Stabilization with two or more rare-earth oxides

Meng *et al.* [110, 116–117] showed that the fcc structure in the Bi_2O_3-based solid solutions with two rare-earth oxide dopants could be stabilized down to room temperature, with much lower content of double dopant oxides than that of a single oxide. This cooperative effect was attributed to the increase in entropy of the resulting ternary system as a consequence of mixing. The transition of a highly symmetric structure stable at high temperatures into a lower symmetry structure stable at low temperatures would be accompanied by a significant entropy change. Based on this thermodynamic argument, these investigators envisaged that it is favourable for the high-temperature fcc phase to be "frozen" at low temperatures. A general observation made by these authors is that the presence of the second dopant in smaller concentration, retained the fcc structure and also resulted in an increase in conductivity, especially in the lower temperature regions. The conductivity, however, was shown to decrease as the second dopant content increases. This behaviour for the $(Bi_2O_3)_{0.76}(Y_2O_3)_{0.24-x}(Gd_2O_3)_x$ system was explained in terms of the appearance of a second phase (probably the rhombohedral) with lower conductivity. The conductivity of the fcc solid solutions containing mixed dopants was found to increase with temperature for a given composition. In addition, the oxygen transference number also showed an increase with increasing dopant content as well as with the temperature for $x < 0.1$. This trend is typified in Table II which shows data for $(Bi_2O_3)_{1-2x}(Y_2O_3)_x(Pr_2O_{11/3})_x$.

TABLE II Transference numbers for $(Bi_2O_3)_{1-2x}(Y_2O_3)_x(Pr_2O_{11/3})_x$ solid solutions

Temperature (°C)	Transference number, $t_{O^{2-}}$			
	$x = 0.075$	$x = 0.100$	$x = 0.125$	$x = 0.150$
500	0.6971	0.7481	0.9844	0.9987
700	0.5903	0.6680	0.9955	0.9986

Hu *et al.* [118] reported the conductivity variation in Bi_2O_3-based oxides doped with mixed rare-earth oxides. The dopant consisted of a raw lanthanide oxide material, containing as many as seven rare-earth metals, whose composition was: Gd(7.5 mol %), Tb (7.5 mol %), Dy (37.5 mol %), Ho (12.4 mol %), Er (18.8 mol %), Tm (4.9 mol %) and Yb (12.3 mol %). The mole fraction (x) of the mixed rare-earth oxide dopant ranged from 0.05–0.80. Their high-temperature XRD and DTA results indicated that the limits for the single fcc phase field were $0.15 < x < 0.51$. This is clearly manifested in the conductivity plots shown in Fig. 9, for various levels of dopant concentration. For example, curve a ($x = 0.05$) shows two distinct knees: one at $\sim 350\,°C$ and the other at $\sim 650\,°C$. The first knee could be due to the monoclinic to rhombohedral transition, while the other to the rhombohedral to cubic one at higher temperature. With increasing dopant concentration (curve b and so on), the low-temperature discontinuity in the conductivity versus temperature plot disappears, giving an approximate lower limit of the mixed oxide dopant concentration, necessary for stabilizing the rhombohedral phase down to below 300 °C. For the solid solutions containing rare-earth oxides in the range $x = 0.15$–0.20, the inflexion in the conductivity plots

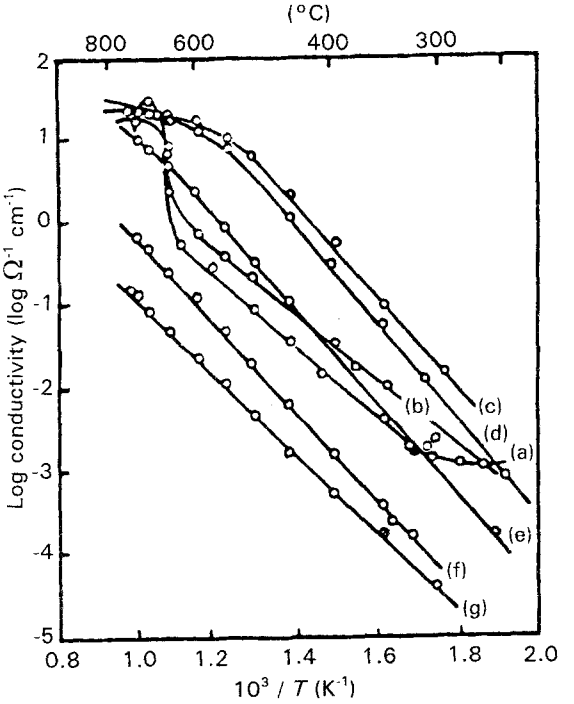

Figure 9 Temperature dependence of conductivities of $(Bi_2O_3)_{1-x}$(mixed-$RE_2O_3)_x$ solid solutions [118]. x: (a) 0.05, (b) 0.10, (c) 0.15, (d) 0.20, (e) 0.33, (f) 0.60, (g) 0.80.

TABLE III Conductivity characteristics of some of the typical solid oxide electrolytes

Electrolyte	Conductivity ($\Omega^{-1}\,cm^{-1}$)		Transference number $t_{O^{2-}}$
	500 °C	700 °C	
$(Bi_2O_3)_{0.8}(Er_2O_3)_{0.2}$	2.2	87.1	0.98
$(Bi_2O_3)_{0.715}(Dy_2O_3)_{0.28}$	0.744	15.1	0.98
$(Bi_2O_3)_{0.75}(Y_2O_3)_{0.25}$	0.013	0.16	0.97
$(Bi_2O_3)_{0.65}(Gd_2O_3)_{0.35}$	0.005	0.1	0.95
$(ZrO_2)_{0.85}(CaO)_{0.15}$	7.1×10^{-4}	5.5×10^{-3}	1.00
$(ZrO_2)_{0.91}(Y_2O_3)_{0.09}$	4.6×10^{-4}	4.5×10^{-3}	1.00

occurs at about 550 °C, which we may recall, is akin to that observed in the simple alkaline-earth as well as single and double rare-earth oxide-doped Bi_2O_3 solid solutions. Hu *et al.* extrapolated the speculation of Meng *et al.* [110], that this behaviour is due to the order–disorder transition of the oxygen vacancies; the higher binding energy of the RE–O bonds compared to that of Bi–O bonds in the structure, contributes to the oxygen ion conduction in the low-temperature region.

It is evident from Fig. 9 that the solid solution having the nominal composition $(Bi_2O_3)_{0.85}(RE_2O_3)_{0.15}$ exhibited the highest conductivity up to the order–disorder transition temperature. The sample $(Bi_2O_3)_{0.80}(RE_2O_3)_{0.20}$ showed higher conductivity in the temperature range above the transition. Comparison of the typical conductivity values in the mixed rare-earth oxide-stabilized Bi_2O_3 with those listed in Table III, for some of the most promising candidate materials, readily shows that while these are comparable or marginally higher than those in $(Bi_2O_3)_{0.715}(Dy_2O_3)_{0.285}$ system, the values are much lower than those reported in the erbia-doped solid solutions. At 700 °C, the conductivities are $(Bi_2O_3)_{0.85}(Dy_2O_3)_{0.15}$ 15.1 $\Omega^{-1}\,cm^{-1}$, $(Bi_2O_3)_{0.85}(RE_2O_3)_{0.15}$ 20.0 $\Omega^{-1}\,cm^{-1}$ and $(Bi_2O_3)_{0.85}(Er_2O_3)_{0.15}$ 87.1 $\Omega^{-1}\,cm^{-1}$.

2.3. Bi_2O_3–M_2O_5 (M = V, Nb, Ta) system

A number of phase equilibria and electrical conductivity investigations has been carried out in the Bi_2O_3–M_2O_5 systems. The phase diagram published by Levin and Waring [119] was recently revised by Powers [88], particularly with respect to the structure of the C′ phase (subsequently designated δ′ by Powers), and the position of the tie line at ~ 605 °C. She investigated the phase relationships and measured the electrical conductivity, in solid solutions containing up to 25 mol % Nb_2O_5, using XRD, DTA and two- and four-probe d.c. conductivity techniques. Pure fcc phase has not been observed at higher concentrations of Nb_2O_5. The revised phase diagram in the Bi_2O_3–Nb_2O_5 system for compositions ⩽ 24 mol % Nb_2O_5 is shown in Fig. 10. Though Levin and Roth [120] suggested that an fcc phase, analogous to that in Bi_2O_3–Nb_2O_5 could exist in the Bi_2O_3–V_2O_5 system, they did not propose a detailed phase diagram.

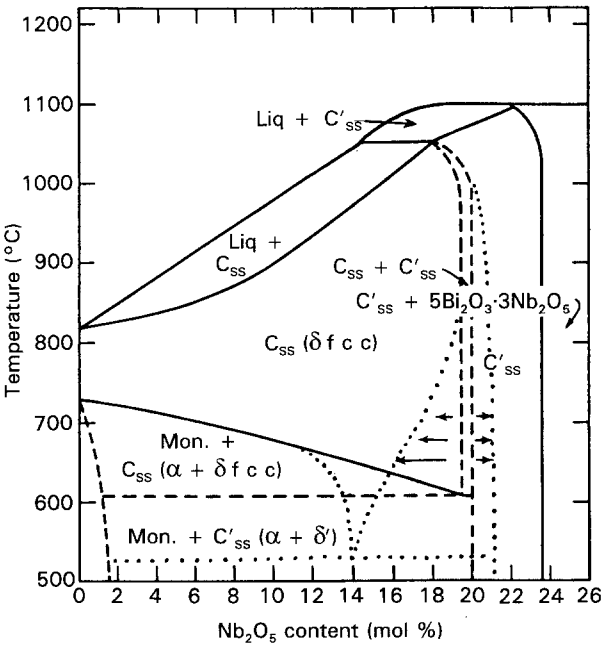

Figure 10 Revised phase diagram for the Bi_2O_3–Nb_2O_5 system for compositions ⩽ 24 mol % Nb_2O_5 [88]. (– – –, ——) Levin and Waring [119].

Recently, Abraham *et al.* [121] predicted high ionic conduction in the compound $Bi_4V_2O_{11}$ ($2Bi_2O_3 \cdot V_2O_5$). This compound has a layered structure and undergoes several structural transitions between 405 °C and the congruent melting point, 887 °C. Takahashi *et al.* [122] and Takahashi and Iwahara [85] investigated the electrical conductivity characteristics in the vanadia (5–20 mol %)-, niobia (5–30 mol %)- and tantala (3–33 mol %)-stabilized bismuth oxide solid solutions, over a wide temperature range. Recently, Meng *et al.* [110], Watanabe [86] and Joshi *et al.* [79] also studied the phase stability and oxygen ion conductivity in pentavalent cation-stabilized Bi_2O_3 solid solutions. According to Takahashi *et al.* [85, 122], the best oxide ion conductor among the Bi–Nb oxides was $(Bi_2O_3)_{0.85}(Nb_2O_5)_{0.15}$ with conductivity comparable to that found in $(Bi_2O_3)_{0.75}(Y_2O_3)_{0.25}$ (Tables III and IV). However, the conductivity data of Powers showed a maximum at 9 mol % Nb_2O_5. She reported conductivity values for $(Bi_2O_3)_{0.85}(Nb_2O_5)_{0.15}$ which are an order of magnitude lower than those given by Takahashi *et al.*, Meng *et al.* and Joshi *et al.* While the agreement among the latter

TABLE IV Conductivity Values of Nb_2O_5-stabilized Bi_2O_3 electrolytes

Electrolyte	Conductivity ($\Omega^{-1}\,cm^{-1}$)		Transference number, $t_{O^{2-}}$	Reference
	500 °C	700 °C		
$(Bi_2O_3)_{0.85}(Nb_2O_5)_{0.15}$	0.011	0.19	0.99	[122]
$(Bi_2O_3)_{0.85}(Nb_2O_5)_{0.15}$	0.017[a]	0.04	–	[79]
$(Bi_2O_3)_{0.80}(Nb_2O_5)_{0.20}$	0.0012	0.019	0.90	[110]
$(Bi_2O_3)_{0.91}(Nb_2O_5)_{0.09}$	0.018	–	–	[86]
$(Bi_2O_3)_{0.85}(Nb_2O_5)_{0.15}$	0.006	–	–	[88]

[a] At 600 °C.

groups of investigators was excellent at 500 °C, they differed quite appreciably at 700 °C, as seen from Table IV. Based on the time dependence of the decay in current density under an applied d.c. voltage, Joshi *et al.* concluded that the niobia-stabilized electrolytes were preferable for applications at 650 °C or lower, to the more conducting yttria-stabilized ones, because the decay of current density in the former was lower.

From the Arrhenius plots (log σ–$1/T$) in the Bi_2O_3–M_2O_5 systems, Takahashi *et al.* concluded that the minimum content of the pentavalent dopant, needed to stabilize the single-phase fcc in the corresponding solid solution was 12.5 mol % for V_2O_5, 15 mol % for Nb_2O_5 and 18 mol % for Ta_2O_5. Thus, it appears that the threshold concentration of the dopant for the stabilization of δ-phase is a function of atomic number of the pentavalent metal. Incidentally, according to these authors, these values correspond to the lower composition limit of the fcc solid solution ranges at least for Nb_2O_5 and Ta_2O_5; in the Bi_2O_3–V_2O_5 system, the fcc phase was not recognized as being single phase over the investigated range of composition. The single-phase fcc structure is stable over 15–25 mol % Nb_2O_5 and 18–25 mol % Ta_2O_5 [110, 122]. On the contrary, Powers suggested that the solid solutions containing 10–14 mol % Nb_2O_5 were only δ, while those in the range 15–21 mol % Nb_2O_5 were mainly δ but also contained the δ′ (structurally similar to δ) phase. The similarity in structure between the two phases creates some difficulty in distinguishing δ from δ′. At this juncture it is worth mentioning that Joshi *et al.* [79] also reached a similar conclusion that niobia-stabilized bismuth oxide, though primarily cubic, might be a mixture of two cubic solid solutions of slightly differing lattice parameters.

However, Watanabe [86] reported that the fcc phase could not be stabilized by adding Nb_2O_5 or Ta_2O_5 to Bi_2O_3. In the Bi_2O_3-rich region of the Bi_2O_3–Ta_2O_5 system, a β-Bi_2O_3 (metastable modification) type phase appeared around ~ 2 mol % Ta_2O_5 [117]; at 8 mol % Ta_2O_5, an fcc phase was identified. Both these phases have been reported to form limited solid solutions and tend to decompose upon annealing. Watanabe, therefore, concluded that the δ-Bi_2O_3 phase cannot be stabilized by a single oxide addition.

From the foregoing discussion, it is clear that the phase relationships in the pseudobinary Bi_2O_3–M_2O_5 systems are not quite clear and somewhat reliable conductivity data are available only in the niobia-stabilized Bi_2O_3 solid solutions. However, because the conductivity values in the fcc phase in this system also are at best comparable to the yttria-stabilized Bi_2O_3, which in turn are much inferior to the erbia analogues, any further research in the Bi_2O_3–M_2O_5 systems would be of only academic interest and no significant technological advantage could be achieved.

2.4. Bi_2O_3–RE_2O_3–Nb_2O_5 (RE = Y, Sm) system

As pointed out in Section 2.2.2, Meng *et al.* [110] observed that the addition of two dopants instead of one seems to exert a cooperative effect in stabilizing the fcc structure in Bi_2O_3-based solid solutions down to room temperatures, with much lower concentration of the two dopants combined. Apart from using two rare-earth oxide dopants, they have also studied the systems Bi_2O_3–Y_2O_3–Nb_2O_5 and Bi_2O_3–Sm_2O_3–Nb_2O_5. In two groups of samples, $(Bi_2O_3)_{0.8}(Y_2O_3)_x(Nb_2O_5)_{0.2-x}$ ($x = 0 - 0.15$) and $(Bi_2O_3)_{0.75}(Y_2O_3)_x(Nb_2O_5)_{0.25-x}$ ($x = 0.00$–0.20), all the solid solutions were found to be single-phase fcc. Based on the conductivity–temperature behaviour of these samples it was concluded that a total amount of yttria and niobia as low as 20 mol % was sufficient to stabilize the δ-phase, while maintaining the high conductivity. The best sample in the Bi_2O_3–Y_2O_3–Nb_2O_5 system was of the composition $(Bi_2O_3)_{0.8}(Y_2O_3)_{0.1}(Nb_2O_5)_{0.1}$, having the conductivity values of 0.014 and 0.19 $\Omega^{-1}\,cm^{-1}$ at 500 and 700 °C, respectively. However, the oxygen ion transference number measurements in the solid solutions $(Bi_2O_3)_{0.75}(Y_2O_3)_x(Nb_2O_5)_{0.25-x}$ in the temperature range 500–800 °C, are contradictory to the above mentioned observations. The latter data clearly show that the sample designated as $(Bi_2O_3)_{0.75}(Y_2O_3)_{0.20}(Nb_2O_5)_{0.05}$ was essentially an ionic conductor ($t_{O^{2-}} \sim 1.0$) in the entire temperature range ($t_{O^{2-}}$ is the transference number). Thus from these investigations it would be rather appropriate to conclude that the solid solution 0.75 Bi_2O_3–0.25 (Y_2O_3 + Nb_2O_5) might be the best choice in this system in terms of the conductivity, especially at higher temperatures. The conductivity of the $(Bi_2O_3)_{0.84}(Sm_2O_3)_{0.04}(Nb_2O_5)_{0.12}$ solid solution was found to be even higher, compared to pure yttria- or pure niobia-doped bismuth oxide samples.

Powers [88] studied the phase equilibria and conduction characteristics in the Bi_2O_3–Y_2O_3–Nb_2O_5 system in the composition range 0–24 mol % dopant. The isothermal section of the phase diagram at 550 °C is shown in Fig. 11. Its most prominent feature is the wide range of solid solution. The solid solution containing the single-phase δ-structure lies predominantly above ~ 15 mol % total dopant. Within the cubic field between 3 and 9 mol % niobia, the presence of an unknown minor phase was detected, whose concentration remained rather constant over the entire range of composition mentioned above. Powers outlined three likely possibilities for the occurrence of the second-phase impurity: (i) transition to superionic conductor at temperature near or below 550 °C, (ii) order/disorder transition, and (iii) instrumental artefact or presence of foreign impurities in the sample.

Powers showed that the highest conductivity value was observed for the sample containing 12 mol % (yttria + niobia) and was virtually constant for 12–15 mol % dopant. This is nearly half as much as reported by Meng *et al.* [110], for the best conducting solid solution in this system. Moreover, the higher niobia compositions showed substantially lower conductivity than the compositions containing comparable amounts of yttria. However, because these measurements were made by the two-probe technique at relatively low temperatures (200–400 °C), it may not be possible to extrapolate these data to higher temperatures without significant errors. It is, therefore, worthwhile to carry out the conductivity measurements afresh, in the composition range mentioned above, over the temperature region 500–900 °C. Powers' work also identified the incompatibility of Bi_2O_3–Y_2O_3–Nb_2O_5 solid solutions with platinum electrodes, under prolonged heating in air.

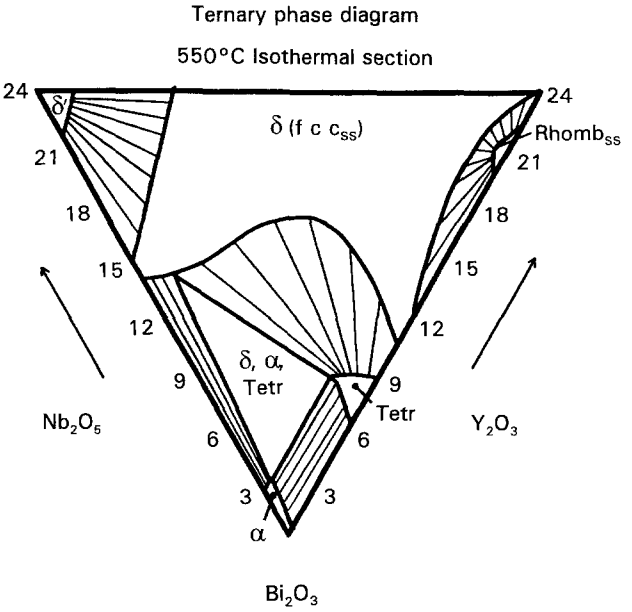

Figure 11 Equilibrium diagram for the Bi_2O_3–Y_2O_3–Nb_2O_5 ternary at 550 °C [88].

2.5. Bi_2O_3–MO_3 (M = W, Mo) system

According to the latest phase diagram, published by Hoda and Chang [123], four intermediate phases exist: $7B_2O_3 \cdot WO_3$ (12.5 mol % WO_3), $7Bi_2O_3 \cdot 2WO_3$ (22.2 mol % WO_3), $Bi_2O_3 \cdot WO_3$ (50.0 mol % WO_3) and $Bi_2O_3 \cdot 2WO_3$ (66.7 mol % WO_3). The $7Bi_2O_3 \cdot WO_3$ is a tetragonal phase which transforms to the fcc structure at 784 °C, while $7Bi_2O_3 \cdot 2WO_3$ has the δ-Bi_2O_3-type fcc structure and forms an extensive range of solid solutions (up to ~ 32 mol % WO_3 at 965 °C). The remaining two compounds are orthorhombic. Gal'perin *et al.* [124] reported that the fcc phase was stable in the compositions from $(Bi_2O_3)_{0.67}(WO_3)_{0.33}$ to $(Bi_2O_3)_{0.78}(WO_3)_{0.22}$ over a wide range of temperatures. On the other hand, Watanabe *et al.* [125] recently reported that the solid solution containing 22.2 mol % WO_3, in fact crystallizes in a tetragonal symmetry and has a limited solid solution range of 21.3–26.3 mol % WO_3 at 700 °C, as opposed to the observation of Hoda and Chang, who earlier assigned an fcc symmetry to this composition. Watanabe [86] argued that because this tetragonal unit cell consisted of psuedo-fcc subcells, it was erroneously identified as the stabilized δ-phase in the X-ray diffraction pattern.

Takahashi and Iwahara [126] investigated the ionic conduction in the sintered oxides of $(Bi_2O_3)_{1-x}(WO_3)_x$, $(0.05 \leqslant x \leqslant 0.50)$. Exceptionally high oxygen ion conductivity was observed in the phase $3Bi_2O_3 \cdot WO_3$, which had the fcc structure over a wide range of temperature, up to at least 850 °C, and its solid solution $((Bi_2O_3)_{0.78}(WO_3)_{0.22}$ at ~ 700 °C). The conductivities in $(Bi_2O_3)_{0.78}(WO_3)_{0.22}$ were typically 0.01 and 0.15 $\Omega^{-1}cm^{-1}$ at 500 and 880 °C respectively. The single-phase fcc structure could be stabilized at $x \geqslant 0.20$ over the range 400–900 °C. Solid solutions containing up to 14.3 mol % WO_3, showed significant hysteresis in the log σ–$1/T$ plots, due to the transformation from monoclinic to cubic structure, as was evinced in other cases too, as a general feature of stabilized δ-Bi_2O_3 solid solutions in the lower regime of dopant concentration. The oxygen ion transference number was very close to unity for the specimen having single δ-phase over a wide range of temperature (600–800 °C), and was almost independent of oxygen pressure, when the latter was varied between 1 and 10^{-6} atm at the anode. It was concluded that $(Bi_2O_3)_{0.76}(WO_3)_{0.24}$ was essentially an oxide ion conductor at 600 °C, even under a $p_{O_2} \sim 10^{-15}$ atm. However, at higher temperatures, the phase was prone to be reduced under low p_{O_2}, such as CO/CO_2 mixtures. This may result in the onset of considerable electronic conduction.

Takahashi *et al.* [127] investigated the ionic conduction in the system Bi_2O_3–MoO_3 in the composition range 20–50 mol % MoO_3. Unlike the fcc phase in Bi_2O_3–WO_3 system discussed above, the tetragonal single phase was found to be stable in the range 22–28 mol % MoO_3. Accordingly, in this composition range the tetragonal phase is the conducting phase. Over the range of 30 to ~ 45 mol % MoO_3, the structure was found to be predominantly mono-

clinic and conductivity was somewhat lower, compared to that in the tetragonal phase.

2.6. Other Bi_2O_3-based systems

Frit *et al.* [128, 129], Demina and Dolgikh [130] and Kikuchi *et al.* [131] studied the phase equilibria in Bi_2O_3–TeO_2, while Mercurio *et al.* [94] determined the compositional domains of several solid solutions in Bi_2O_3–RE_2O_3–TeO_2 systems. Based on the results of these investigations, both the compositional domains and the crystallographic characteristics within the Bi_2O_3–TeO_2 system seem to depend strongly on the synthesis temperature, thermal treatment and p_{O_2} in the ambient. Kikuchi *et al.* showed that the δ-Bi_2O_3-type fcc phase (which extended up to 40 mol % TeO_2) could be quenched, but below 700 °C, it decomposes into α-Bi_2O_3 and a new compound $Bi_6Te_2O_{15}$ ($3Bi_2O_3 \cdot 2TeO_3$) having an orthorhombic structure. No conductivity data have yet been reported in the Bi_2O_3–TeO_2 system.

Recently, Bloom *et al.* [132] reported to have synthesized new compounds in Bi_2O_3–Al_2O_3 and Bi_2O_3–La_2O_3–Al_2O_3 systems and tested them in oxygen concentration cells in the range 500–800 °C. Undoped $Bi_2Al_4O_9$ was found to have an intrinsic conductivity of 0.01 $\Omega^{-1}\,cm^{-1}$ at 800 °C. The compound $La_{0.7}Bi_{0.3}AlO_3$ containing 5 mol % Zn has been shown to have high conductivities, of the order of 0.1 $\Omega^{-1}\,cm^{-1}$ at 800 °C.

3. Conclusion

Bismuth sesquioxide-based solid electrolytes have higher conductivity than the conventional and more popular stabilized zirconia systems, in the temperature region of contemplated operation of solid oxide fuel cells. One of the most striking features of this family of electrolytes is that doping with an oxide of practically any stable valency metal in the periodic table (barring the actinides) appears to stabilize the much sought after δ (fcc)-phase. Several high oxygen ion conducting compositions in various systems have been identified. These materials can serve as solid electrolytes in fuel cell devices, provided that allied problems, such as the compatibility with interconnector materials, stability with respect to the electrode materials, stability with respect to the fuel environment, etc., are addressed. However, the instability of the bismuth oxide-based electrolytes under moderate reducing atmosphere may seriously limit their applications in fuel cell environments. Owing to rather easy transition into various other crystallographically different phases in different temperature regions as well as upon ageing at a given temperature, mechanical instability of the electrolyte made out of these materials may also pose challenges in real applications. Usage of composite electrolytes based on the stabilized bismuth oxide material with a thin coating of YSZ seems to be the ultimate solution to avoid degradation of the former in long-term applications, without significantly affecting the overall conductivity across the YSZ membrane. It is also surprising to note that in all the research efforts on Bi_2O_3-based oxide electrolyte systems, no systematic attempt has been reported in the literature, to determine or even estimate the electrolytic domain boundaries for the most promising candidate materials by constructing the classical three-dimensional log σ–logp_{O_2}–$1/T$ Patterson diagrams. It would be worthwhile to generate these diagrams for p_{O_2} ranging from 1 atm to that corresponding to CO/CO_2 and/or H_2/H_2O mixture in the temperature range 500–900 °C. Also, the toughening of the electrolyte can be achieved by precipitation of a second phase in the electrolyte. This additional phase might enhance the conductivity as well, as is the case with the alumina-toughened TZP electrolytes. Finally, experiments are needed to be carried out with stabilized bismuth oxide electrolytes in simulated and actual fuel cell configurations over extended periods of time. This exercise would enable the researchers to estimate and then improve the shelf-life of this material by compositing with more stable zirconia films.

References

1. "Proceedings of the Grove Anniversary Fuel Cell Symposium", Royal Institution, London, 18–21 September 1989 (Elsevier, Amsterdam, 1990).
2. S. SRINIVASAN, F. J. SALZANO and A. R. LANDGREBE (eds), "Industrial Water Electrolysis", (The Electrochemical Society, Princeton, NJ, 1978).
3. K. KENDAL, *Am. Ceram. Soc. Bull.* **70** (1991) 1159.
4. N. Q. Minh, *Chemtech.* **21** (1991) 32.
5. *Idem. ibid.* **21** (1991) 120.
6. B. C. H. STEELE, I. KELLY, H. MIDDLETON and R. RUDKIN, *Solid State Ionics* **28–30** (1988) 1547.
7. D. C. FEE and J. P. ACKERMAN, Fuel Cell Seminar, Courtesy Associates, Washington DC (1983) p. 11.
8. H. BINDER, A. KOEHLING, A. KRUPP, K. RICHTER and G. SANDSTEDE, *Electrochim. Acta* **8** (1963) 781.
9. T. H. ETSELL and S. N. FLENGAS, *Chem. Rev.* **70** (1970) 339.
10. Y. L. SANDLER, *J. Electrochem. Soc.* **118** (1977) 1378.
11. N. J. MASKALICK and C. C. SUN, *ibid.* **118** (1977) 1386.
12. H. S. ISAACS, in "Advances in Ceramics", Vol. 3, "Science and Technology of Zirconia" edited by A. H. Heuer and L. W. Hobbs (The American Ceramic Society, Columbus, OH, (1981) p. 406.
13. O. YAMAMOTO, Y. TAKEDA, R. KANNO and M. NODA, in "Advances in Ceramics". Vol. 24 "Science and Technology of Zirconia III", edited by S. Somiya (The American Ceramic Society, Columbus, OH, 1988) p. 829.
14. S. F. PALGUEV, V. K. DILDERMAN and A. D. NEUIMIN, *J. Electrochem. Soc.* **122** (1975) 745.
15. K. S. GOTO and W. PLUSCHKELL, in "Physics of Electrolytes", vol. 2, edited by J. Hladik (Academic Press, London, 1972) p. 540.
16. T. TAKAHASHI, *ibid.*, p. 989.
17. P. KOFSTAD, "Nonstoichiometry, Diffusion and Electrical conductivity in Binary Metal Oxides" (Wiley Interscience, New York, 1972).
18. H. L. TULLER and A. S. NOWICK, *J. Electrochem. Soc.* **122** (1975) 255.
19. R. T. DIRSTINE, R. N. BLUMENTHAL and T. F. KUECH, *ibid.* **126** (1979) 264.
20. T. KUDO and H. OBAYASHI, *ibid.* **122** (1975) 142.
21. D. Y. WANG and A. S. NOWICK, *J. Solid State Chem.* **35** (1980) 325.
22. R. G. ANDERSON and A. S. NOWICK, *Solid State Ionics* **5** (1981) 547.
23. H. YAHIRO, K. EGUCHI and H. ARAI, *ibid.* **21** (1986) 37.
24. P. N. ROSS Jr. and T. G. BENJAMIN, *J. Power Sources* **1** (1976/1977) 311.

25. D. S. TANNHAUSER, *J. Electrochem. Soc.* **125** (1978) 1277.
26. H. YAHIRO, Y. BABA, E. EGUCHI and H. ARAI, *ibid.* **135** (1988) 2077.
27. W. WEPPNER and H. SCHUBERT, in "Advances in Ceramics", Vol. 24, "Science and Technology of Zirconia III", edited by S. Somiya (The American Ceramic Society, Columbus, OH, (1988) p. 837.
28. T. SATO, M. ISHITSUKA, T. FUKUSHIMA, T. ENDO and M. SCHIMADA, *Mater. Sci. Forum* **34–36** (188) 189.
29. B. Y. LIAW and W. W. WEPPNER, *J. Electrochem. Soc.* **138** (1991) 2478.
30. J. DRENNAN and S. P. S. BADWAL, in "Advances in Ceramics", Vol. 24B, "Science and Technology of Zirconia III", edited by S. Somiya, N. Yamamoto and H. Hanagida (The American Ceramic Society, Columbus, OH, 1988) p. 807.
31. B. C. H. STEELE, in "High Conductivity Solid Ionic Conductors: Recent Trends and Applications", edited by T. Takahashi (World Scientific, Singapore, 1989) p. 402.
32. K. TSUKUMA and M. SCHIMADA, *J. Mater. Sci.* **20** (1985) 1178.
33. N. KHAN and B. C. H. STEELE, *Mater. Sci. Eng.* **B8** (1991) 265.
34. A. P. SELLAR and B. C. H. STEELE, *Mater. Sci. Forum* **34–36** (1988) 255.
35. R. L. COOK, R. C. MacDUFF and A. F. SAMMELLS, *J. Electrochem. Soc.* **137** (1990) 3309.
36. R. L. COOK and A. F. SAMMELLS, *Solid State Ionics* **45** (1991) 311.
37. A. F. SAMMELLS, R. L. COOK, J. H. WHITE, J. J. OSBORNE and R. C. MacDUFF, *ibid.* **52** (1992) 111.
38. R. L. COOK, J. J. OSBORNE, J. H. WHITE, R. C. MacDUFF and A. F. SAMMELLS, *J. Electrochem. Soc.* **139** (1992) L19.
39. J. B. GOODENOUGH, A. MANTHIRAM, M. PARANTHAMAN and Y. S. ZHEN, *Mater. Sci. Eng.* **B12** (1992) 357.
40. B. C. H. STEELE, *ibid.* **B12** (1992) 79.
41. I. KONTOULIS and B. C. H. STEELE, *J. Eur. Ceram. Soc.* **9** (1992) 459.
42. M. SCHWARTZ, B. F. LINK and A. F. SAMMELLS, *J. Electrochem. Soc.*, **140** (1993) L62.
43. H. IWAHARA, T. ESAKA, H. UCHIDA and N. MAEDA, *Solid State Ionics* **3–4** (1981) 359.
44. H. IWAHARA, H. UCHIDA, K. KONDO and K. OGAKI, *J. Electrochem. Soc.* **135** (1989) 529.
45. H. IWAHARA, H. UCHIDA, K. OGAKI and H. NAGATO, *ibid.* **138** (1991) 295.
46. B. HEED and A. LUNDEN, Technical Report to the Swedish Board of Technical Development, Sweden (1972).
47. A. LUNDEN, B.-E. MELLANDER and B. ZHU, *Acta Chem. Scand.* **45** (1991) 981.
48. L. G. SILLEN, *Ark. Kemi Mineral Geol.* **12A** (1937) 1.
49. W. C. SCHUMB and E. S. RITTER, *J. Am. Chem. Soc.* **65** (1943) 1055.
50. G. GATTOW and Z. SCHUETZE, *Anorg. Allg. Chem.* **318** (1962) 176.
51. *Idem, ibid.* **328** (1964) 44.
52. C. N. R. RAO, G. V. SUBBARAO and S. RAMDAS, *J. Phys. Chem.* **73** (1969) 672.
53. H. A. HARWIG, *Z. Anorg. Allg. Chem.* **444** (1978) 151.
54. H. A. HARWIG and J. W. WEENK, *ibid.* **444** (1978) 111.
55. T. TAKAHASHI (ed.), "High Conductivity Solid Ionic Conductors: Recent Trends and Applications", (World Scientific, Singapore, 1989) p.1.
56. P. O. BATTLE, C. R. A. CATLOW, J. W. HEAP and L. M. MORONEY, *J. Solid State Chem.* **63** (1986) 8.
57. A. V. VIRKAR, J. NACHLAS, A. V. JOSHI and J. DIAMOND, *J. Am. Ceram. Soc.* **73** (1990) 3382.
58. K. Z. FUNG and A. V. VIRKAR, *ibid.* **74** (1991) 1970.
59. A. V. VIRKAR, *J. Electrochem. Soc.* **138** (1991) 1481.
60. T. TAKAHASHI, T. ESAKA and H. IWAHARA. *J. Appl. Electrochem.* **7** (1977) 299.
61. E. M. LEVIN and R. S. ROTH, *J. Res. Nat. Bur. Stand.* **68A** (1964) 199.
62. T. TAKAHASHI, H. IWAHARA and T. NAGAI, *J. Appl. Electrochem.* **2** (1972) 97.
63. P. CONFLANT, J. C. BOIVIN and D. THOMAS, *J. Solid State Chem.* **18** (1976) 133.
64. L. G. SILLEN and B. SILLEN, *Z. Phys. Chem.* **49B** (1944) 27.
65. L. G. SILLEN and B. AURIVILLIUS, *Z. Krystallogr.* **101** (1939) 483.
66. P. CONFLANT, J. C. BOIVIN and D. THOMAS, *J. Solid State Chem.* **35** (1980) 192.
67. A. D. NEUIMIN, L. D. YUSHINA, YU. M. OVCHINNIKOV and S. F. PALGUEV, in "Transactions of the Institute of Electrochemistry 4", Urals Academy of Sciences, Electrochemistry of Molten and Solid Electrolytes, Vol. 2 (translated from Russian), edited by M. V. Smirnov (Consultant Bureau, New York, 1964) p. 92.
68. K. HAUFFE and H. PETERS, *Z. Phys. Chem.* **201** (1952) 121.
69. T. TAKAHASHI, T. ESAKA and H. IWAHARA, *J. Solid State Chem.* **16** (1976) 317.
70. T. SUZUKI, Y. DANSUI, T. SHIRAI and C. TSUBAKI, *J. Mater. Sci.* **20** (1985) 3125.
71. H. D. BAEK and A. V. VIRKAR, *J. Electrochem. Soc.* **138** (1992) 3174.
72. K. Z. FUNG, H. D. BAEK and A. V. VIRKAR, *Solid State Ionics* **52** (1992) 199.
73. M. J. VERKERK and A. J. BURGGRAAF, *J. Appl. Electrochem.* **10** (1980) 677.
74. T. TAKAHASHI, H. IWAHARA and T. ARAO, *ibid.* 5 (1975) 187.
75. T. TAKAHASHI, T. ESAKA and H. IWAHARA, *ibid.* **7** (1977) 299.
76. J. H. W. de WIT, T. HONDERS and G. H. J. BROERS, in "Fast Ion Transport in Solids", edited by P. Vashishta, J. N. Mundy and G. K. Shenoy (North Holland, Amsterdam, 1979) p. 657.
77. W. N. LAWLESS and S. L. SWARTZ, *Phys. Rev. B* **28** (1983) 2125.
78. C. WANG, X. XU and B. LI, *Solid State Ionics* **13** (1983) 135.
79. A. V. JOSHI, S. KULKARNI, J. NACHLAS, J. DIAMOND and N. WEBER, *J. Mater. Sci.* **25[2B]** (1990) 1237.
80. A. WATANABE and T. KIKUCHI, *Solid State Ionics* **21** (1986) 287.
81. K. KRUIDHOF, K. J. DE VRIES and A. J. BURGGRAAF, *ibid.* **37** (1990) 213.
82. P. J. DODOR, J. TANAKA and A. WATANABE, *ibid.* **25** (1987) 177.
83. E. M. LEVIN and R. S. ROTH, *J. Res. Nat. Bur. Stand.* **68A** (1964) 200.
84. R. K. DATTA and J. P. MEEHAN, *Z. Anorg. Allg. Chem.* **383** (1971) 328.
85. T. TAKAHASHI and H. IWAHARA, *Mater. Res. Bull.* **13** (1978) 1447.
86. A. WATANABE, *Solid State Ionics* **40–41** (1990) 882.
87. E. M. LEVIN and R. S. ROTH, *J. Res. Nat. Bur. Stand.* **68A** (1964) 197.
88. V. J. POWERS, PhD thesis, Ohio State University (1989).
89. T. TAKAHASHI, H. IWAHARA and Y. NAGAI, *J. Appl. Electrochem.* **2** (1972) 97.
90. T. TAKAHASHI and H. IWAHARA, *ibid.* **3** (1973) 65.
91. M. J. VERKERK and A. J. BURGGRAAF, *Solid State Ionics* **3–4** (1981) 463.
92. P. DURAN, J. R. JURADO, C. MOURE, N. VALVERDE and B. C. H. STEELE, *Mater. Chem. Phys.* **18** (1987) 287.
93. J. R. JURADO, C. MOURE, P. DURAN and N. VALVERDE, *Solid State Ionics* **28–30** (1988) 518.
94. D. MERCURIO, M. EL FARISSI, B. FRIT, J. M. REAU and J. SENEGAS, *ibid.* **39** (1990) 297.
95. A. WATANABE, *ibid.* **35** (1989) 281.
96. T. TAKAHASHI, T. ESAKA and H. IWAHARA, *J. Appl. Electrochem.* **5** (1975) 197.
97. P. SU and A. V. VIRKAR, *J. Electrochem. Soc.* **139** (1992) 1671.
98. M. J. VERKERK and A. J. BURGGRAAF, *ibid.* **128** (1981) 75.

99. S. N. NASANOVA, V. SEREBENNIKOV and G. A. NARNOV, *Russ. J. Inorg. Chem.* **18** (1973) 1244.
100. M. J. VERKERK, K. KEIZER and A. J. BURGGRAAF, *J. Appl. Electrochem.* **10** (1980) 81.
101. M. J. VERKERK, M. W. J. HAMMINK and A. J. BURGGRAAF, *J. Electrochem. Soc.* **130** (1983) 70.
102. K. KEIZER, M. J. VERKERK and A. J. BURGGRAAF, *Ceramurg. Int.* **5** (1979) 143.
103. H. KRUIDHOF, K. SESHAN, G. M. H. van de VELDE, K. J. de VRIES and A. J. BURGGRAAFF, *Mater. Res. Bull.* **23** (1988) 371.
104. M. DUMELIE, G. NOWOGROCKI and J. C. BOIVIN, *Solid State Ionics* **28–30** (1988) 524.
105. I. C. VINKE, J. L. BAKIEWICZ, B. A. BOUKAMP, K. J. de VRIES and A. J. BURGGRAAF, *ibid.* **40–41** (1990) 886.
106. I. C. VINKE, S. SESHAN, B. A. BOUKAMP, K. J. de VRIES and A. J. BURGGRAAF, *ibid.* **34** (1989) 235.
107. R. D. SHANNON, *Acta Crystallogr.* **A32** (1976) 751.
108. H. T. CAHEN, T. G. M. van der BELT, J. W. H. de WIT and G. H. J. BROERS, *Solid State Ionics* **1** (1980) 411.
109. A. WATANABE, *ibid.* **34** (1989) 35.
110. G. MENG, C. CHEN, X. HAN, P. YANG and D. PENG, *ibid.* **28–30** (1988) 533.
111. A. V. VIRKAR and M. R. PLICHTA, *J. Am. Ceram. Soc.* **66** (1983) 451.
112. T. C. YUAN and A. V. VIRKAR, *ibid.* **69** (1986) C 310.
113. *Idem, ibid.* **71** (1988) 12.
114. D. DROBECK, A. V. VIRKAR and R. M. COHEN, *J. Phys. Chem. Solids* **51** (1990) 977.
115. S. J. KIM, Z. C. CHEN and A. V. VIRKAR, *J. Am. Ceram. Soc.* **71** (1988) C 428.
116. G. MENG, M. ZHOU and D. PENG, *J. Chin. Silicate Soc.* **13** (1985) 366.
117. G. MENG, C. YU and D. PENG, *J. China Univ. Sci. Tech. Suppl.* **15** (1985) 225.
118. K. HU, C. CHEN, D. PENG and G. MENG, *Solid State Ionics* **28–30** (1988) 566.
119. E. M. LEVIN and T. L. WARING, *J. Res. Nat. Bur. Stand.* **66A** (1962) 451.
120. E. M. LEVIN and R. S. ROTH, *ibid.* **68A** (1964) 202.
121. F. ABRAHAM, M. F. DUBREUILLE-GRESSE, G. MAIRESSE and G. NOWOGROCKI, *Solid State Ionics* **28–30** (1988) 529.
122. T. TAKAHASHI, H. IWAHARA and T. ESAKA, *J. Electrochem. Soc.* **124** (1977) 1563.
123. S. N. HODA and L. L. Y. CHANG, *J. Am. Ceram. Soc.* **57** (1974) 323.
124. E. L. GAL'PERIN, L. YA. ERMAN, I. K. KOLCHIN, M. A. BELOVA and K. S. CHERNYSHEV, *Russ. J. Inorg. Chem.* **11** (1966) 1137.
125. A. WATANABE, N. ISHIZAWA and M. KATO, *J. Solid State Chem.* **60** (1985) 252.
126. T. TAKAHASHI and H. IWAHARA, *J. Appl. Electrochem.* **3** (1973) 65.
127. T. TAKAHASHI, T. ESAKA and H. IWAHARA, *ibid.* **7** (1977) 31.
128. B. FRIT, M. JAYMES, G. PEREZ and P. HAGENMULLER, *Rev. Chim. Min.* **8** (1971) 453.
129. B. FRIT and M. JAYMES, *ibid.* **9** (1972) 873.
130. L. A. DEMINA and V. A. DOLGIKH, *Russ. J. Inorg. Chem.* **29** (1984) 547.
131. T. KIKUCHI, Y. KITAMI, M. YOKOYAMA and H. SAKAI, *J. Mater. Sci.* **24** (1989) 4275.
132. I. BLOOM, M. C. HASH, J. P. ZEBROWSKI, K. M. MYLES and K. KRUMPLET, *Solid State Ionics* **53–56** (1992) 739.

Received 3 August 1993
and accepted 16 February 1994